Steel and Composite Structures, *Vol. 21, No. 1 (2016) 1-36*
DOI: http://dx.doi.org/10.12989/scs.2016.21.1.001

Nonlinear magneto-electro-mechanical vibration analysis of double-bonded sandwich Timoshenko microbeams based on MSGT using GDQM

M. Mohammadimehr* and S. Shahedi

Department of Solid Mechanics, Faculty of Mechanical Engineering, University of Kashan, Kashan, Iran

(*Received November 22, 2015, Revised January 26, 2016, Accepted February 26, 2016*)

Abstract. In the present study, the nonlinear magneto-electro-mechanical free vibration behavior of rectangular double-bonded sandwich microbeams based on the modified strain gradient theory (MSGT) is investigated. It is noted that the top and bottom sandwich microbeams are considered with boron nitride nanotube reinforced composite face sheets (BNNTRC-SB) with electrical properties and carbon nanotube reinforced composite face sheets (CNTRC-SB) with magnetic fields, respectively, and also the homogenous core is used for both sandwich beams. The connections of every sandwich beam with its surrounding medium and also between them have been carried out by considering Pasternak foundations. To take size effect into account, the MSGT is introduced into the classical Timoshenko beam theory (CT) to develop a size-dependent beam model containing three additional material length scale parameters. For the CNTRC and BNNTRC face sheets of sandwich microbeams, uniform distribution (UD) and functionally graded (FG) distribution patterns of CNTs or BNNTs in four cases FG-X, FG-O, FG-A, and FG-V are employed. It is assumed that the material properties of face sheets for both sandwich beams are varied in the thickness direction and estimated through the extended rule of mixture. On the basis of the Hamilton's principle, the size-dependent nonlinear governing differential equations of motion and associated boundary conditions are derived and then discretized by using generalized differential quadrature method (GDQM). A detailed parametric study is presented to indicate the influences of electric and magnetic fields, slenderness ratio, thickness ratio of both sandwich microbeams, thickness ratio of every sandwich microbeam, dimensionless three material length scale parameters, Winkler spring modulus and various distribution types of face sheets on the first two natural frequencies of double-bonded sandwich microbeams. Furthermore, a comparison between the various beam models on the basis of the CT, modified couple stress theory (MCST), and MSGT is performed. It is illustrated that the thickness ratio of sandwich microbeams plays an important role in the vibrational behavior of the double-bonded sandwich microstructures. Meanwhile, it is concluded that by increasing H/lm, the values of first two natural frequencies tend to decrease for all amounts of the Winkler spring modulus.

Keywords: smart materials; nonlinear vibration analysis; double-bonded sandwich Timoshenko microbeams; size effect; MSGT; GDQM

*Corresponding author, Assistant Professor, E-mail: mmohammadimehr@kashanu.ac.ir

http://www.techno-press.org/?journal=scs&subpage=6 ISSN: 1229-9367 (Print), 1598-6233 (Online)

1. Introduction

Sandwich structures are being used extensively in aerospace, marine, naval, transportation and civil engineering industries. Due to their special characteristics, sandwich structures are being considered as primary and secondary structural members. Some of superior qualities of sandwich structures consist of: high strength and stiffness to weight ratio, ease of manufacturing, thermal and acoustic insulation, and flexibility in design. The widespread range and importance of these applications, represents the necessary of accurate model capable of predicting the vibration response of sandwich structures. Some researches of this structures subjected to mechanical loading are denoted in the literature including Plantema (1966), and Reissner (1948). Many classical researches on sandwich structures such as Allen (1969), Zenkert (1995) and Vinson (1999) considered that the core material is vertically incompressible. Liew *et al*. (2015) performed mechanical analysis of functionally graded carbon nanotube reinforced composites (FG-CNTRC) and illustrated a review of various investigations in the existing literature in terms of static, free vibration, dynamic, buckling and non-linear analyses of FG-CNTRC. Static and dynamic analysis of FG Euler–Bernoulli microbeam was investigated by Kahrobaiyan *et al*. (2012) based on strain gradient theory (SGT). Tajalli *et al*. (2013) performed mechanical behavior analysis of size-dependent micro-scaled FG Timoshenko beams by SGT. Zhang *et al*. (2014) considered non-classical Timoshenko beam element based on the SGT and revealed that lower size effects are significant when the beam thickness is small, but become negligible with increasing beam thickness.

Some researchers have been worked about optimization of nanostructures and its applications and also to determine the optimal distribution of carbon nanotubes for specific purposes. Nanthakumar *et al*. (2015) presented shape and topology optimization of nanostructures using a coupled XFEM/Level set method and investigated a computational method for the optimization of nanostructures, where our specific interest is in capturing and elucidating surface stress and surface elastic effects on the optimal nanodesign, they obtained results of optimal topologies of a nanobeam subject to cantilever and fixed boundary conditions. Also, they showed that the importance of size and aspect ratio in determining how surface effects impact the optimized topology of nanobeams. Ghasemi *et al*. (2014a) and (2015) studied optimum fiber content and distribution in fiber-reinforced solids using a reliability and NURBS based sequential optimization approach and concluded that when system unreliability increases, fiber distribution optimization becomes more influential. In the other work, Ghasemi *et al*. (2014b) focused on the uncertainties propagation and their effects on reliability of polymeric nanocomposite (PNC) continuum structures using stochastic multi-scale modeling, in the framework of the combined geometry and material optimization.

In recent years, static, buckling, and free vibration behavior of sandwich structure has been widely investigated by some researchers. The vibration and buckling of FG sandwich beams based on a quasi-3D theory has been performed by Vo *et al*. (2015). Grygorowicz *et al*. (2015) studied the elastic buckling of a sandwich beam with variable mechanical properties of the core. They compared the values of the obtained critical load by the analytical and numerical methods. The free vibration of the FG sandwich beams by a mesh-free boundary-domain integral equation method was analyzed by Yang *et al*. (2014). Their results demonstrated that the current developed method is not only convenient to implement, but also showed higher accuracy, convergence and efficiency. Lanc *et al*. (2015) investigated buckling analysis of thin-walled FG sandwich beams and expressed that the power-law index and skin-core-skin thickness ratios play very important

role on the buckling analysis of sandwich beams. Rahmani and co-workers (2009) exhibited free vibration analysis of sandwich structures with a flexible FG syntactic core. They concluded that the eigen-frequenies of the beam decrease with an increase in the *l*/*h* ratio. Free vibration analysis of sandwich cylindrical panel with FG core using three-dimensional theory of elasticity was discussed by Alibeigloo and Liew (2014). Wang and Shen (2011, 2012) illustrated nonlinear vibration and bending of sandwich plates with nanotube-reinforced composite face sheets. Bui *et al*. (2013) studied transient responses and natural frequencies of sandwich beams with FG core. Based on Mori-Tanaka approach, the free vibration of sandwich beam with FG core by using the element free Galerkin method was studied by Chehel Amirani *et al*. (2009). Vo *et al*. (2014) investigated vibration and buckling of sandwich beams with FG skins homogeneous core using a refined shear deformation theory. In the other work, static analysis of higher order sandwich beams by weak form quadrature element method was carried out by Wang and Wang (2014) and also showed that the proposed beam element can yield very accurate displacements and stresses as compared to theoretical solutions. Damanpack and Khalili (2012) represented high-order free vibration analysis of sandwich beams with a flexible core using dynamic stiffness method and revealed that the dynamic stiffness method with small number of elements in solving the eigenvalue problem has a good accuracy in the other result.

The classical continuum elasticity theory cannot descript the accurate structural behavior at micro and nano scale because of lacking of the material length scale parameter. Therefore, during past years, several non-classical higher-order continuum theories have been introduced and employed to predict size-dependent responses of micro-scaled structures. One of the size-dependent continuum theories is SGT, introduced by Fleck and Hutchinson (1993). After that, Lam *et al*. (2003) proposed a MSGT with three material length scale parameters relevant to dilatation gradient, deviatoric gradient and symmetric rotation gradient tensors. In recent years, this theory has been utilized by many researchers to analyze the static and dynamic problems of micro-scale structures. For instance, static bending and free vibration behaviors of Euler-Bernoulli and Timoshenko homogeneous microbeams have been respectively developed by Kong *et al*. (2009) and Wang *et al*. (2010). Using SGT and MCST, the bending, buckling and free vibrations of Euler-Bernoulli microbeams have been employed by Akgöz and Civalek (2011, 2012, 2013a). Moreover, a new size-dependent sinusoidal shear deformation beam model based on SGT was proposed by them Akgöz and Civalek (2013b). Sahmani *et al*. (2014) studied nonlinear free vibration analysis of FG third-order shear deformable microbeams based on the MSGT and demonstrated that by approaching from metal phase to ceramic phase for an FGM microbeam, the linear frequency and nonlinear frequency ratio tend to decrease and increase, respectively. Mohammadimehr *et al*. (2015a) studied the vibration analysis of visco-elastic tapered micro-rod based on SGT resting on visco-Pasternak foundation using differential quadrature method (DQM). Lei and co-workers (2013) analyzed bending and vibration of FG sinusoidal microbeams based on the SGT and showed that the FG microbeams exhibit significant size-dependence when the thickness of the microbeam approached to the material length scale parameter. Electro-thermal vibration of visco-elastically coupled BNNT systems conveying fluid embedded on elastic foundation via SGT have been carried out by Ghorbanpour Arani and Amir (2013). Size-dependent bending, buckling and free vibration of FG Timoshenko microbeams based on the most general SGT has been conducted by Ansari *et al*. (2013). Also, in other work, Ansari *et al*. (2011) represented free vibration analysis of size-dependent FG microbeams based on the strain gradient Timoshenko beam theory and it is observed that the value of gradient index play an important role in the vibrational response of the microbeams of lower slenderness ratios. Mohammadimehr *et al*. (2015b) analyzed free vibration

of viscoelastic double-bonded polymeric nanocomposite plates reinforced by FG-CNTs using MSGT, sinusoidal shear deformation theory and meshless method and showed that the elastic foundation, vdW interaction and magnetic field increase the dimensionless natural frequency of the double-bonded nanocomposite plates for CT, MCST and MSGT. Also, in the other work (Mohammadimehr *et al*. 2016b), they investigated modified strain gradient Reddy rectangular plate model for biaxial buckling and bending analysis of double-coupled piezoelectric polymeric nanocomposite reinforced by FG-CNT and concluded that the elastic foundation and van der Waals interaction in contrast to applied voltage increase the dimensionless critical biaxial buckling load and vice versa decrease the dimensionless deflection of the double-coupled nanocomposite plates. Electro-elastic analysis of a sandwich thick plate considering FG core and composite piezoelectric layers on Pasternak foundation using third-order shear deformation theory was performed by Mohammadimehr *et al*. (2016a) and concluded that the natural frequency and critical buckling load diminish with an increase in the power law index. In other study, a new Euler-Bernoulli beam model based on a simplified SGT and its applications was presented by Liang *et al*. (2014). The obtained numerical results showed the significance of the Poisson's effect and the strain gradient elastic effect. The improved high order analysis of sandwich beams by considering a bilinear elasto-plastic behavior of core was investigated by Jedari Salami *et al*. (2015). A simple shear deformation theory for thermo-mechanical behavior of FG sandwich plates on elastic foundations was introduced by Taibi *et al*. (2015). A new simple shear and normal deformations theory for FG beams was presented by Bourada *et al*. (2015). Interfacial shear stress optimization in sandwich beams with polymeric core using non-uniform distribution of reinforcing ingredients was performed by Ghasemi *et al*. (2014c). They illustrated that adding reinforcements homogeneously into polymers will slightly improve the interfacial shear stress but that considerable improvements are observed when the distribution of the reinforcement in the core is optimized. Bouremana and co-workers (2013) expressed a new first shear deformation beam theory based on neutral surface position for FG beams by assuming that the in-plane and transverse displacements consist of bending and shear components. A new nonlinear high order theory for sandwich beams along with an analytical and experimental investigation was expressed by Dariushi and Sadighi (2013). They indicated that nonlinear effects become more significant in some cases and the results of linear model are unreliable.

The objective of the current study is to investigate the nonlinear magneto-electro-mechanical free vibration behavior of rectangular double-bonded sandwich beams including sandwich beam with carbon nanotube reinforced composite (CNTRC) face sheets including magnetic field and sandwich beam with boron nitride nanotube reinforced composite (BNNTRC) face sheets consisting of electrical properties based on the MSGT. Considering homogenous core for both sandwich beams and assuming connection of every sandwich beam with its surrounding medium and also between them by Pasternak foundation, the MSGT is introduced into the classical Timoshenko beam theory to develop a size-dependent beam model. For the CNTRC and BNNTRC face sheets of sandwich beams, uniform distribution (UD) and four functionally graded distribution patterns of CNTs or BNNTs including FG-A, FG-V, FG-O, and FG-X are considered. It is assumed that the material properties of face sheets for both sandwich beams are varied in the thickness direction and estimated through the extended rule of mixture. By using Hamilton's principle, the size-dependent nonlinear governing differential equations of motion together with corresponding boundary conditions are derived. Afterward, by employing GDQM, the higher-order equations of motion are discretized to calculate first two natural frequencies of double-bonded sandwich beams.

2. Material properties of double-bonded sandwich beams

Sandwich structures represent a special form of a layered structure that consist of two thin stiff and strong face sheets separated by a relatively thick, lightweight, and homogenous core material. Fig. 1 shows two sandwich microbeams are bounded together and are attached with Pasternak foundation from both sides. It is assumed that the homogenous core of two sandwich beams are made of pure aluminum metal and face sheets of upper and lower sandwich beams are made of FG-BNNTRC and FG-CNTRC, respectively, with different distributions of BNNT and CNT in the thickness direction. In this paper, it is assumed that there is no delamination between the core and face sheets of both sandwich beams. Herein after, the lower and upper sandwich beams with FG-CNTRC and FG-BNNTRC face sheets, respectively, have been determined by sub or super-scripts "C" and "B" representing the sandwich beam with CNTRC and BNNTRC face sheets, respectively. The length of two sandwich beams denote L, and thicknesses of face sheets and the core of CNTRC are h_f^C and h_c^C, respectively and similarly for BNNTRC are h_f^B and h_c^B.

The UD and FG distributions (FG-A, FG-V, FG-O and FG-X) of BNNT and CNT in the thickness direction of the face sheets for both sandwich beams respectively, are considered, as shown in Fig. 2. In this figure, the density of BNNT or CNT within the face sheet area is constant and the volume fraction varies through the thickness of the face sheet. The Cartesian coordinate systems (x, y, z) is used on the central axis of each sandwich beam where (x_1, y_1, z_1), (x_2, y_2, z_2) axes are taken along the length, width and height directions of CNTRC and BNNTRC, respectively. The homogenous core of both sandwich beams is modeled as an elastic material that its material properties are constant along the z-axis. The mechanical parameters ρ_c, E_c, G_c, υ_c are denoted the density, Young's modulus, shear modulus and Poisson's ratio of the core, respectively.

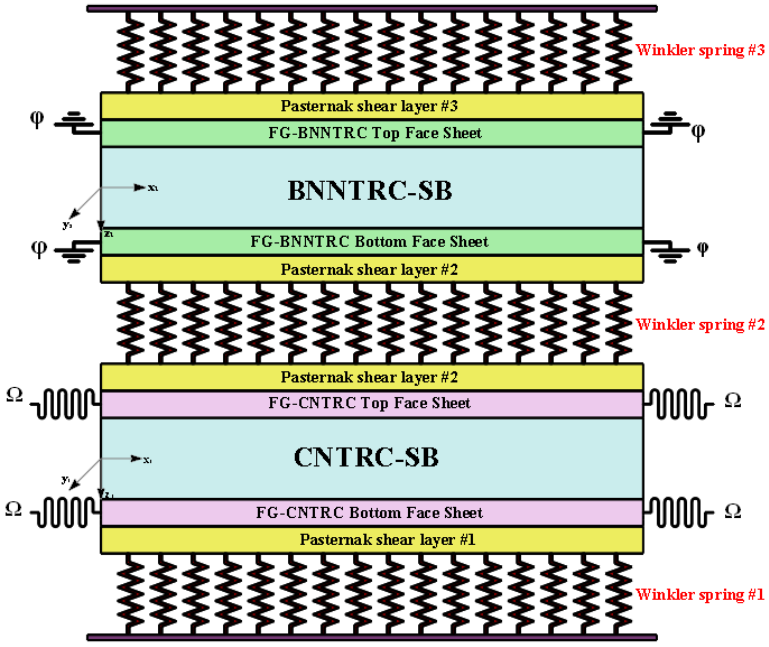

Fig. 1 An schematic view of the double-bonded sandwich Timoshenko microbeams resting on the Pasternak foundation

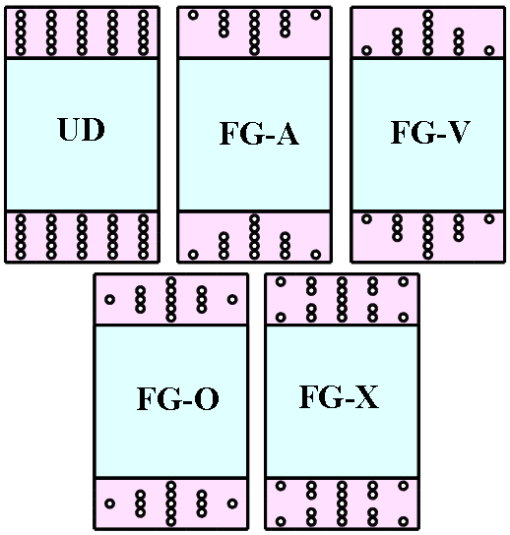

Fig. 2 Configurations of the sandwich microbeam with various CNT or BNNT distribution patterns in face sheets

Here, we first determine the effective material properties of both sandwich beams based on the extended rule of mixture. The material properties of both BNNTRC and CNTRC were shown to be anisotropic by many researchers (Han and Elliott 2007, Zhang and Shen 2006). The effective Young's modulus and shear modulus of CNTRC face sheets through the extended rule of mixture can be written as (Yas and Samadi 2012, Mohammadimehr *et al*. 2016b and c)

$$E_{11f}^{C} = \eta_1 V_{cnt} E_{11}^{cnt} + V_m E_m^{C} \tag{1a}$$

$$\frac{\eta_2}{E_{22f}^{C}} = \frac{V_{cnt}}{E_{22}^{cnt}} + \frac{V_m}{E_m^{C}} \tag{1b}$$

$$\frac{\eta_3}{G_{12}^{f}} = \frac{V_{cnt}}{G_{11}^{cnt}} + \frac{V_m}{G_m^{C}} \tag{1c}$$

where $E_{11}{}^{cnt}$, $E_{22}{}^{cnt}$ and $G_{12}{}^{cnt}$ denote the Young's modulus and shear modulus of CNT, respectively. $E_m{}^{C}$ and $G_m{}^{C}$ indicate the corresponding properties of the matrix for face sheet. The CNT efficiency parameters η_i (i = 1, 2, 3) are introduced in Eq. (1) to consider the size-dependent material properties and will be later determined by matching the elastic moduli of CNTRC obtained through the molecular dynamics (MD) simulations with the obtained numerical results from the rule of mixture. $V_{cnt}{}^{C}$ and $V_m{}^{C}$ are the volume fractions for CNT and matrix, respectively, which are related by $V_{cnt}{}^{C} + V_m{}^{C} = 1$. Similarly, Poisson's ratio υ and mass density ρ of the CNTRC face sheets for bottom sandwich beam can be determined as

$$\upsilon_f^{C} = V_{cnt}\upsilon_{cnt}^{C} + V_m\upsilon_m^{C}, \qquad \rho_f^{C} = V_{cnt}\rho_{cnt}^{C} + V_m\rho_{cnt}^{C} \tag{2}$$

In which $\upsilon_{cnt}{}^{C}$, $\upsilon_m{}^{C}$ denote the Poisson's ratios, and $\rho_{cnt}{}^{C}$, $\rho_m{}^{C}$ are the densities of the CNT and

matrix, respectively. The effective Young's modulus and shear modulus of BNNTRC face sheets for top sandwich beam through the rule of mixture have been denoted as follows

$$E_f^B = V_{bnnt} E_{bnnt}^B + V_m E_m^B \tag{3a}$$

$$G_f^B = V_{bnnt} G_{bnnt}^B + V_m G_m^B \tag{3b}$$

The different distributions of the CNT or BNNT along the thickness direction of the face sheets of sandwich beam depicted in Fig. 2 are assumed to be as follows (Mohammadimehr *et al*. 2016b and c)

$$FG-UD: \quad V_{rc} = V_{rc}^* \tag{4}$$

$$FG-A: \quad V_{rc} = \left(1 + \frac{2z}{h}\right) V_{rc}^* \tag{5}$$

$$FG-V: \quad V_{rc} = \left(1 - \frac{2z}{h}\right) V_{rc}^* \tag{6}$$

$$FG-O: \quad V_{rc} = 2 - 4\frac{|z|}{h} V_{rc}^* \tag{7}$$

$$FG-X: \quad V_{rc} = 4\frac{|z|}{h} V_{rc}^* \tag{8}$$

where V_{rc}^* is the volume fraction of reinforced composite which means BNNT or CNT that is calculated from

$$V_{rc}^* = \frac{W_{rc}}{W_{rc} + (\rho^{rc}/\rho^m)(1 - W_{rc})} \tag{9}$$

W_{rc} is the mass fraction of BNNT or CNT.

3. The double-bonded sandwich Timoshenko beams

With considering the dependency of deformation behavior on the size effects in the microbeams, it is essential to consider size dependent effects in the analysis of the behavior of FG microbeams at micro scale. Conventional continuum mechanics fails to predict the size-dependent response of the structures at micro and nanoscale due to lacking intrinsic length scales. In recent years, several higher-order elasticity theories have been introduced to develop size-dependent continuum models. The SGT was proposed by Lam *et al*. (2003) that introduce additional dilatation gradient tensor and the deviatoric stretch gradient tensor in addition to the symmetric rotation gradient tensor in the MCST of Yang *et al*. (2002). These tensors can be characterized by three independent material length scale parameters (l_0, l_1, l_2) and two classical material constants (E, υ) for isotropic linear elastic materials. After that, the strain energy V for an isotropic linear elastic material occupying region X (with a volume element Ω) is given by

$$V = \frac{1}{2}\int \Omega\left(\sigma_{ij}\varepsilon_{ij} + p_i\gamma_i + \tau_{ijk}^{(1)}\eta_{ijk}^{(1)} + m_{ij}^s\chi_{ij}^s - D_iE_i - B_iH_i\right)dv \tag{10}$$

where ε_{ij}, γ_i, $\eta_{ijk}^{(1)}$, χ_{ij}^s, E_i, H_i represent the strain tensor, the dilatation gradient tensor, the deviatoric stretch gradient tensor, the symmetric rotation gradient tensor, the electric field and magnetic field, respectively which can be defined as (Lam *et al*. 2003)

$$\begin{aligned}
&\varepsilon_{ij} = \frac{1}{2}\left(u_{i,j} + {}_{,i}\right)\\
&\gamma_i = \varepsilon_{mm,i}\\
&\eta_{ijk}^{(1)} = \frac{1}{3}\left(\varepsilon_{jk,i} + \varepsilon_{ki,j} + \varepsilon_{ij,k}\right) - \frac{1}{15}\left[\delta_{ij}\left(\varepsilon_{mm,k} + 2\varepsilon_{mk,m}\right) + \delta_{jk}\left(\varepsilon_{mm,i} + 2\varepsilon_{mi,m}\right) + \delta_{ki}\left(\varepsilon_{mm,j} + 2\varepsilon_{mj,m}\right)\right]\\
&\chi_{ij}^s = \frac{1}{4}\left(e_{ipg}\varepsilon_{qj,p} + e_{jpg}\varepsilon_{qi,p}\right)\\
&H_i = -\Omega_{,i}\\
&E_i = -\varphi_{,i}
\end{aligned} \tag{11}$$

where $\partial_{,i}$ represents differentiation with respect to the x_i. u_i denotes the components of the displacement vector u, ε_{mm} is the dilatation strain. δ_{ij} and e_{ijk} are the Knocker and the alternate symbols, respectively, φ and Ω are the scalar functions of electric potential of BNNTRC-SB and magnetic potential of CNTRC-SB, respectively. The corresponding classical and higher order stress measures for a linear isotropic elastic material can be showed by the following constitutive relations (Lam *et al*. 2003)

$$\begin{aligned}
&\sigma_{ij} = \lambda\delta_{ij}\varepsilon_{kk} + 2G\varepsilon_{ij} - \alpha_T\delta_{ij}\Delta T - h\delta_{ij}E_i\\
&p_i = 2Gl_0^2\gamma_i\\
&\tau_{ijk}^{(1)} = 2Gl_0^2\eta_{ijk}^{(1)}\\
&m_{ij}^s = 2Gl_2^2\chi_{ij}^s\\
&D_x = h_{11}\left(\varepsilon_{xx} - \alpha_T^{BNNTRC}\Delta T\right) - \in_{11}\varphi_{,x}\\
&B_x = q_{11}\left(\varepsilon_{xx} - \alpha_T^{CNTRC}\Delta T\right) - \mu_{11}\Omega_{,x}
\end{aligned} \tag{12}$$

where l_0, l_1 and l_2 denote the additional independent three material length scale parameters associated with dilatation gradients, deviatoric stretch gradients and symmetry rotation gradients, respectively. The dielectric permittivity constant and magnetic permeability constant have been showed by ϵ_{11} and μ_{11}, respectively. The Lame constants λ and G in the constitutive equation of the classical stress σ_{ij} are given by

$$\lambda = \frac{\upsilon E}{(1+\upsilon)(1-2\upsilon)}, \quad G = \frac{E}{2(1+\upsilon)} \tag{13}$$

The kinematics of an arbitrary point in the micro beam based on Timoshenko beam theory can be represented as follows

$$\begin{aligned} U_1(x,z,t) &= U(x,t) + z\Psi(x,t) \\ U_2(x,z,t) &= 0 \\ U_3(x,z,t) &= W(x,t) \end{aligned} \tag{14}$$

in which U, W, Ψ represent the axial displacement of neutral axis, the lateral deflection of the beam and the rotation angle of the normal to the mid-surface of the beam, respectively. Substituting Eq. (14) into Eq. (11), the nonzero components of the von Kármán type nonlinear strain-displacement relations are expressed as

$$\begin{aligned} \varepsilon_{xx} &= \frac{\partial U}{\partial x} + z\frac{\partial \Psi}{\partial x} + \frac{1}{2}\left(\frac{\partial W}{\partial x}\right)^2 \\ \gamma_{xz} &= \frac{\partial W}{\partial x} + \Psi \end{aligned} \tag{15}$$

By inserting Eqs. (14) and (15) into Eq. (11), the following nonzero components of γ, χ^s and $\eta^{(1)}$ and the nonzero components of the classical stress tensor are defined in Appendix A. By substituting Eqs. (A-1) and (A-2) into Eq. (12), the nonzero components of the higher-order stresses can be obtained as given in Appendix B. To derive the governing differential equations of motion, the Hamilton's principle is employed as the following form

$$\delta \prod = \int_0^t (\delta T - \delta V + \delta W)dt = 0 \tag{16}$$

where δV, δW, and δT denote the virtual strain energy, the virtual work done by external forces, and the virtual kinetic energy, respectively. In the following, the total strain energy of double-bonded sandwich beams for both CNTRC-SB and BNNTRC-SB are shown as V^C and V^B that are obtained as follows

$$V^C = \frac{1}{2}\int_0^L \int_\Omega \left(\begin{array}{l} Q_{11}^C \left[\begin{array}{l} \left(\dfrac{\partial U_1}{\partial x} + z\dfrac{\partial \Psi_1}{\partial x} + \dfrac{1}{2}\left(\dfrac{\partial W_1}{\partial x}\right)^2 \right)^2 \\ + \left(\dfrac{q_{11}\Omega_{1,x}}{Q_{11}^C} - \alpha_T^C.\Delta T \right)\left(\dfrac{\partial U_1}{\partial x} + z\dfrac{\partial \Psi_1}{\partial x} + \dfrac{1}{2}\left(\dfrac{\partial W_1}{\partial x}\right)^2 \right) \end{array} \right] \\ + \left[k_s Q_{55}^C \left(\dfrac{\partial W_1}{\partial x} + \Psi_1 \right)^2 \right] + \left[q_{11}\Omega_{1,x}\left(\dfrac{\partial U_1}{\partial x} + z\dfrac{\partial \Psi_1}{\partial x} + \dfrac{1}{2}\left(\dfrac{\partial W_1}{\partial x}\right)^2 - \alpha_T^C.\Delta T \right) \right] \\ + \left[k_1 Q_{55}^C \left(\dfrac{\partial^2 U_1}{\partial x^2} + \dfrac{\partial^2 \Psi_1}{\partial x^2} + \dfrac{\partial W_1}{\partial x}\dfrac{\partial^2 W_1}{\partial x^2} \right)^2 \right] \\ + \left[k_2 Q_{55}^C \left(\dfrac{\partial^2 W_1}{\partial x^2} + 2\dfrac{\partial \Psi_1}{\partial x^2} \right)^2 \right] + \left[k_3 Q_{55}^C \left(\dfrac{\partial \Psi_1}{\partial x} + 2\dfrac{\partial^2 W_1}{\partial x^2} \right)^2 \right] \end{array} \right) dA.dx \tag{17}$$

and

$$V^B = \frac{1}{2}\int_0^L \int_\Omega \left(\begin{array}{l} Q_{11}^B \left[\begin{array}{l} \left(\dfrac{\partial U_2}{\partial x} + z\dfrac{\partial \Psi_2}{\partial x} + \dfrac{1}{2}\left(\dfrac{\partial W_2}{\partial x}\right)^2 \right)^2 \\ + \left(\dfrac{h_{11}\varphi_{2,x}}{Q_{11}^B} - \alpha_T^B.\Delta T \right)\left(\dfrac{\partial U_2}{\partial x} + z\dfrac{\partial \Psi_2}{\partial x} + \dfrac{1}{2}\left(\dfrac{\partial W_2}{\partial x}\right)^2 \right) \end{array} \right] \\ + \left[k_s Q_{55}^B \left(\dfrac{\partial W_2}{\partial x} + \Psi_2 \right)^2 \right] + \left[h_{11}\Omega_{2,x}\left(\dfrac{\partial U_2}{\partial x} + z\dfrac{\partial \Psi_2}{\partial x} + \dfrac{1}{2}\left(\dfrac{\partial W_2}{\partial x}\right)^2 - \alpha_T^B.\Delta T \right) \right] \\ + \left[k_1 Q_{55}^B \left(\dfrac{\partial^2 U_2}{\partial x^2} + \dfrac{\partial^2 \Psi_2}{\partial x^2} + \dfrac{\partial W_2}{\partial x}\dfrac{\partial^2 W_2}{\partial x^2} \right)^2 \right] \\ + \left[k_2 Q_{55}^B \left(\dfrac{\partial^2 W_2}{\partial x^2} + 2\dfrac{\partial \Psi_2}{\partial x^2} \right)^2 \right] + \left[k_3 Q_{55}^B \left(\dfrac{\partial \Psi_2}{\partial x} + 2\dfrac{\partial^2 W_2}{\partial x^2} \right)^2 \right] \end{array} \right) dA.dx \quad (18)$$

where superscripts "*C*" and "*B*" denote the CNTRC-SB and BNNTRC-SB, respectively

$$K_1 = 2l_0^2 + \frac{4}{5}l_1^2, \qquad K_2 = \frac{8}{15}l_1^2, \qquad K_3 = \frac{1}{16}l_2^2 \quad (19)$$

The kinetic energy by T can be defined as

$$\begin{aligned} T &= \frac{1}{2}\int_0^L \int_\Omega \left(\rho \left[\left(\frac{\partial U_1}{\partial t} \right)^2 + \left(\frac{\partial U_2}{\partial t} \right)^2 + \left(\frac{\partial U_3}{\partial t} \right)^2 \right] \right) dA.dx \\ &= \frac{1}{2}\int_0^L \int_\Omega \left(\rho \left[\left(\frac{\partial U}{\partial t} + z\frac{\partial \psi}{\partial t} \right)^2 + \left(\frac{\partial W}{\partial t} \right)^2 \right] \right) dA.dx \end{aligned} \quad (20)$$

And the external work due to surrounding elastic medium, W_q, can be obtained as (Mohammadimehr *et al*. 2010)

$$W_q = \frac{1}{2}\int_0^L \left\{ \begin{array}{l} \left[\left(-k_{w1}W_1 + G_{p1}\dfrac{\partial^2 W_1}{\partial x^2} \right) W_1 \right] \\ + \left[\left(-k_{w2}(W_2 - W_1) + G_{p2}\left(\dfrac{\partial^2 W_2}{\partial x^2} - \dfrac{\partial^2 W_1}{\partial x^2} \right) \right)(W_2 - W_1) \right] \\ + \left[\left(-k_{w3}W_2 + G_{p3}\dfrac{\partial^2 W_2}{\partial x^2} \right) W_2 \right] \end{array} \right\} dx \quad (21)$$

In which ρ and A are the density and the cross-sectional area of every sandwich beam, respectively. The stiffness components and inertia related terms of both sandwich beams can be defined as

$$\begin{aligned}\left(I_{0C}, I_{1C}, I_{2C}\right) &= \int_z \rho^{cntrc}(z)(1, z, z^2)dz \\ \left(I_{0B}, I_{1B}, I_{2B}\right) &= \int_z \rho^{bnntrc}(z)(1, z, z^2)dz\end{aligned} \tag{22}$$

$$\begin{aligned}&\left(A_{11C}, B_{11C}, D_{11C}\right) = \int_z Q_{11}^{cntrc}(z)(1, z, z^2)dz,\ \left(A_{11B}, B_{11B}, D_{11B}\right) = \int_z Q_{11}^{bnntrc}(z)(1, z, z^2)dz, \\ &\left(A_{55C}, B_{55C}, D_{55C}\right) = \int_z Q_{55}^{cntrc}(z)(1, z, z^2)dz,\ \left(A_{55B}, B_{55B}, D_{55B}\right) = \int_z Q_{55}^{bnntrc}(z)(1, z, z^2)dz,\end{aligned} \tag{23}$$

Taking the variation of U_1, W_1, Ψ_1 and Ω_1 for CNTRC-SB and U_2, W_2, Ψ_2 and Φ_2 for BNNTRC-SB by using Eqs. (17)-(21) and according to Eq. (16), the governing equations of motion for both sandwich beams using the clamped-clamped boundary conditions will be obtained that are described in Appendix C.

The dimensionless mechanical, electrical, magnetic, geometric, size effect, elastic foundation parameters are defined as follows

$$\begin{aligned}&\zeta = \frac{x}{L},\ \ \eta = \frac{L}{H},\ \ \left(u_1, u_2, w_1, w_2\right) = \frac{\left(U_1, U_2, W_1, W_2\right)}{H},\ \ \left(\psi_1, \psi_2\right) = \left(\Psi_1, \Psi_2\right), \\ &\tau = \frac{t}{L}\sqrt{\frac{A_{110}}{I_{00}}},\ \ \left(K_{w1}, K_{w2}, K_{w3}\right) = \left(\frac{K_{w1}L^2}{A_{110}},\ \frac{K_{w2}L^2}{A_{110}},\ \frac{K_{w3}L^2}{A_{110}}\right) \\ &\left(G_{p1}, G_{p2}, G_{p3}\right) = \left(\frac{G_{p1}}{A_{110}},\ \frac{G_{p2}}{A_{110}},\ \frac{G_{p3}}{A_{110}}\right), \\ &\left(a_{11C}, a_{55C}, b_{11C}, b_{55C}, d_{11C}, d_{55C}\right) = \left(\frac{A_{11C}}{A_{110}},\ \frac{A_{55C}}{A_{110}},\ \frac{B_{11C}}{A_{110}H},\ \frac{B_{55C}}{A_{110}H},\ \frac{D_{55C}}{A_{110}H^2},\ \frac{D_{55C}}{A_{110}H^2}\right), \\ &\left(a_{11B}, a_{55B}, b_{11B}, b_{55B}, d_{11B}, d_{55B}\right) = \left(\frac{A_{11B}}{A_{110}},\ \frac{A_{55B}}{A_{110}},\ \frac{B_{11B}}{A_{110}H},\ \frac{B_{55B}}{A_{110}H},\ \frac{D_{55B}}{A_{110}H^2},\ \frac{D_{55B}}{A_{110}H^2}\right), \\ &\left(I_{0C}, I_{1C}, I_{2C}\right) = \left(\frac{I_{0C}}{I_{00}},\ \frac{I_{1C}}{I_{00}H},\ \frac{I_{2C}}{I_{00}H^2}\right),\ \ \left(I_{0B}, I_{1B}, I_{2B}\right) = \left(\frac{I_{0B}}{I_{00}},\ \frac{I_{1B}}{I_{00}H},\ \frac{I_{2B}}{I_{00}H^2}\right) \\ &\left(K_1, K_2, K_3\right) = \left(\frac{K_1}{I_{00}},\ \frac{K_2}{I_{00}H},\ \frac{K_3}{I_{00}H^2}\right),\ \ h_{11} = \frac{h_{11}^2 h_f}{L \in_{11} A_{110}},\ \ \hat{q}_{11} = \frac{q_{11}^2 h_f}{L\mu_{11}A_{110}}\end{aligned} \tag{24}$$

In which A_{110} and I_{00} denote the values of A_{11} and I_0 for a homogeneous matrix beam. Substituting Eq. (24) into Eqs. (C-1) and (C-2), the dimensionless governing equations of motion for both sandwich beams are derived that are illustrated in Appendix D.

4. Solution method

Different numerical techniques can be employed to solve the governing equations and associated boundary conditions. In this study, GDQM (Shu 2000, Shu and Du 1997) is used to discretize the governing differential equations of motion. The GDQM has been proved to be an efficient higher-order numerical technique for the solution of boundary value problems with respect to other numerical technique and has been widely used to achieve acceptable solutions for various dynamic and stability problems and different boundary conditions. Since this numerical method provides simple and low computational cost. Moreover, the implementation of the GDQM is relatively easier and the efforts needed for solving the problem with GDQM is also relatively less in comparison to the other numerical methods. The advantages of the GDQM included no restriction on the number of grid points used for the approximation and the weighted coefficients are determined using simple recurrence relation instead of solving a set of linear algebraic equations as in other version of DQM. In this method, the partial derivative of a function with respect to spatial variables at a given discrete point are approximated as a weighted linear sum of the function values at all discrete points chosen in the solution domain. Thus the partial derivatives of a function f at a point x_i are expressed as

$$\left.\frac{d^n f}{dx^n}\right|_{x=x_i} = \sum_{j=1}^{N} C_{ij}^{(n)} f\left(x_j\right) \tag{25}$$

where $C_{ij}^{(n)}$ are the respective weighting coefficients matrix, N is the number of grid points and f can be taken as U, W, Ψ. The weighting coefficients for the first derivative (i.e., $n = 1$) are

$$C_{ij}^{(n)} = \begin{cases} \prod_{k=1,k\neq i,j}^{N} \left(x_i - x_k\right) \Big/ \prod_{k=1,k\neq j}^{N} \left(x_j - x_k\right) & (i \neq j) \\ \prod_{k=1,k\neq i}^{N} \dfrac{1}{\left(x_i - x_k\right)} & (i = j) \end{cases} \qquad i, j = 1, 2, \ldots, N \tag{26}$$

For higher-order derivatives, we have

$$\begin{aligned} C_{ij}^{(2)} &= \sum_{k=1}^{N} C_{ik}^{(1)} C_{kj}^{(1)} \\ C_{ij}^{(3)} &= \sum_{k=1}^{N} C_{ik}^{(1)} C_{kj}^{(2)} = \sum_{k=1}^{N} C_{ik}^{(2)} C_{kj}^{(1)} \\ C_{ij}^{(4)} &= \sum_{k=1}^{N} C_{ik}^{(1)} C_{kj}^{(3)} = \sum_{k=1}^{N} C_{ik}^{(3)} C_{kj}^{(1)} \end{aligned} \tag{27}$$

Through the procedure of discretizing the problem, the grid points are generated as according to Chebyshev-Gauss-Lobatto pattern as (Shu and Du 1997)

$$x_j = \frac{1}{2}\left\{1 - \cos\left[\frac{\pi(i-1)}{N-1}\right]\right\}, \quad i = 1, 2, \ldots, N \tag{28}$$

5. Numerical results

In this section, based on MSGT, numerical results are presented for determination of first two dimensionless nonlinear natural frequencies of double-bonded sandwich beams (Fig. 1) including the lower sandwich beam with CNTRC face sheets and the upper sandwich beam with BNNTRC face sheets resting on Pasternak foundation. It should be mentioned that letting the material length scale parameters l_0, l_1, l_2 equal to zero, the governing equations modeled by the classical theory (CT) will be achieved. Also, setting the material length scale parameters l_0 and l_1 to zero, the present model reduces to the MCST. Afterward, numerical results corresponding to each type of beam theory are obtained and compared together. The material properties of homogenous core for both sandwich beams, made of pure aluminum metal, are considered as follows

$$E_c = 70\,\text{GPa}, \quad \upsilon_c = 0.33, \quad \rho_c = 2780\,\text{kg/m}^3 \tag{29}$$

For top and bottom face sheets of CNTRC-SB with similar wall thickness, poly methyl methacrylate (PMMA) and CNTs are considered as the matrix and reinforcement, respectively, where their material properties at room temperature (300 *K*) are assumed to be as the following form (Yas and Samadi 2012)

$$\begin{aligned}
&E_m^C = 2.5\,\text{GPa}, \;\; \upsilon_m^C = 0.3, \;\; \rho_m^C = 1190\,\text{kg/m}^3, \;\; \alpha_m^C = 45e-6,\\
&E_{11}^{cnt} = 600\,\text{GPa}, \;\; E_{22}^{cnt} = 10\,\text{GPa}, \;\; G_{12}^{cnt} = 17.2\,\text{GPa}, \;\; \upsilon_{cnt}^C = 0.19,\\
&\rho_{cnt}^C = 1400\,\text{kg/m}^3, \;\; \alpha_{cnt}^C = 3.4587e-6, \;\; V_{cnt}^* = 0.12,\\
&\eta_1 = 1.2833, \quad \eta_2 = \eta_3 = 1.0556
\end{aligned} \tag{30}$$

where the CNT efficiency parameters are evaluated through matching the obtained Young's modulli E_{11}, E_{22} and shear modulus G_{12} of CNTRC from the extended rule of mixture to ones predicted from MD simulations (Han and Elliott 2007, Griebel and Hamaekers 2004). Considering BNNTs as reinforcement and Polyvinylidene fluoride (PVDF) as matrix of face sheets for BNNTRC-SB, their material properties at room temperature are defined as follows (Salehi-Khojin and Jalili 2008, Ghorbanpour Arani *et al*. 2015)

$$\begin{aligned}
&E_m^B = 1.1\,\text{GPa}, \;\; \upsilon_m^B = 0.3, \;\; \rho_m^B = 1750\,\text{kg/m}^3, \;\; \alpha_m^B = 7.1e-5,\\
&h_{11M}^B = 0.135, \;\; \in_0 = 8.854185E-12, \;\; \in_{11m}^B = 1250 * \in_0, \;\; E_{bnnt}^B = 1800\,\text{GPa},\\
&\upsilon_{bnnt}^B = 0.34, \;\; \rho_{bnnt}^B = 3487\,\text{kg/m}^3, \;\; \alpha_{bnnt}^B = 1.2e-6,\\
&h_{11bnnt}^B = 0.95, \quad \in_{11bnnt}^B = 20 * \in_0
\end{aligned} \tag{31}$$

Moreover, the other parameters for CNTs and PMMA have been estimated as follows

$$\begin{aligned}
&\mu_0 = 8.854185e-12, \quad q_{11m}^C = 0.135,\\
&\mu_{11m}^C = 1250 * \mu_0, \quad q_{11cnt}^C = 0.95, \quad \mu_{11cnt}^C = 20 * \mu_0
\end{aligned} \tag{32}$$

The constant parameters in the following text are in accordance to Table 1. A parametric study has been performed and typical results are shown in Table 2 and Figs. 3-15. The first two

dimensionless nonlinear frequencies of double-bonded sandwich beams for various distribution types of Winkler spring modulus corresponding to different slenderness ratio are listed in Table 2. It is revealed that for different slenderness ratio, the values of k_{w1} have most influence on the first

Table 1 The constant parameters in the present work

Core-to-face sheet thickness ratio of both sandwich beams $\left(\frac{h_{core}}{h_f^C}\right)$ or $\left(\frac{h_{core}}{h_f^B}\right)$		Dimensionless Winkler modulus (k_w)	Dimensionless Pasternak shear modulus (G_p)	Slenderness ratio (L/H)
3		0.1	0.02	15
Height of sandwich beams (H)	Temperature change (ΔT)	Material length scale parameter (l_m/H)	CNT or BNNT volume fraction $\left(V^*_{CNT} \text{ or } V^*_{BNNT}\right)$	
10 μm	50 C	0.5	0.12	

Table 2 The effect of Winkler spring modulus on the nonlinear frequency of double-bonded sandwich microbeams

	$L/H = 10$		$L/H = 20$		$L/H = 30$	
(k_{w1}, k_{w2}, k_{w3})	Freq. 1	Freq. 2	Freq. 1	Freq. 2	Freq. 1	Freq. 2
(0.1, 0.1, 0.1)	1.1447	1.5193	0.8430	1.2194	0.7316	1.1392
(0.1, 0.1, 0.05)	1.1404	1.5039	0.8282	1.2062	0.7113	1.1271
(0.1, 0.1, 0.2)	1.1523	1.5503	0.8685	1.2476	0.7665	1.1656
(0.05, 0.1, 0.1)	1.1209	1.5158	0.8198	1.2088	0.7082	1.1256
(0.2, 0.1, 0.1)	1.1895	1.5273	0.8833	1.2434	0.7710	1.1694
(0.1, 0.05, 0.1)	1.1360	1.4855	0.8419	1.1695	0.7315	1.0848
(0.1, 0.2, 0.1)	1.1576	1.5876	0.8445	1.3139	0.7317	1.2408

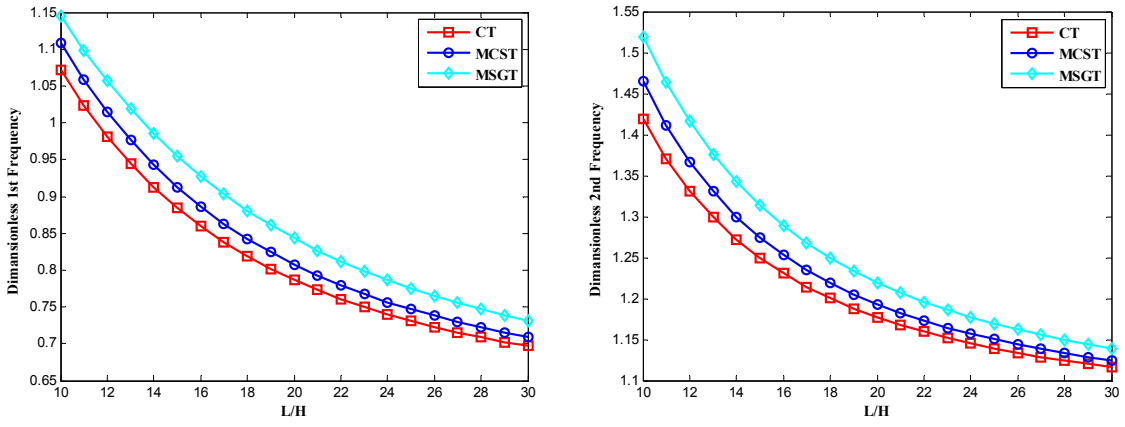

(a) (b)

Fig. 3 The effect of slenderness ratio on the nonlinear frequency of double-bonded sandwich microbeams for various theories of size dependent effect: (a) 1st frequency; (b) 2nd frequency

(1st) natural frequency in comparison to other cases, but the second (2nd) natural frequency has been highly affected with the k_{w2} value. In other words, the extreme values of 1st and 2th natural frequencies can be yielded with varying k_{w1} and k_{w2}, respectively.

Fig. 3 shows the variation of first two dimensionless natural frequencies of double-bonded sandwich beams versus slenderness ratio based on three theories of various size dependent effects such as CT, MCST and MSGT. It can be seen that although first two frequencies of double-bonded sandwich beams decrease by increasing the slenderness ratio, but in a certain slenderness ratio, the obtained frequencies for MSGT and CT beam models predict the maximum and minimum values of natural frequencies, respectively, among the various beam models. Moreover, it can be observed from these figures that the natural frequency of double-bonded sandwich Timoshenko beams for

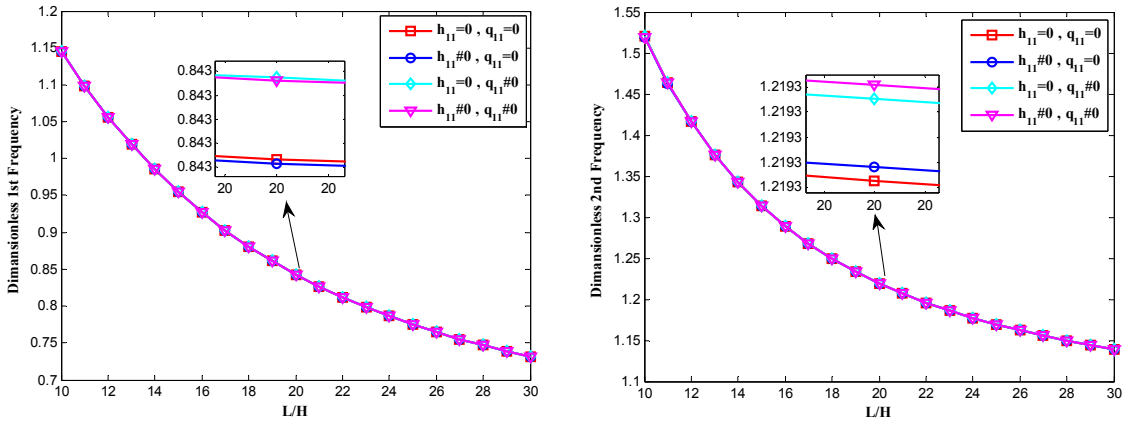

(a) (b)

Fig. 4 The effect of electric and magnetic fields of BNNTRC and CNTRC on the nonlinear frequency of double-bonded sandwich microbeams versus slenderness ratio: (a) 1st frequency; (b) 2nd frequency

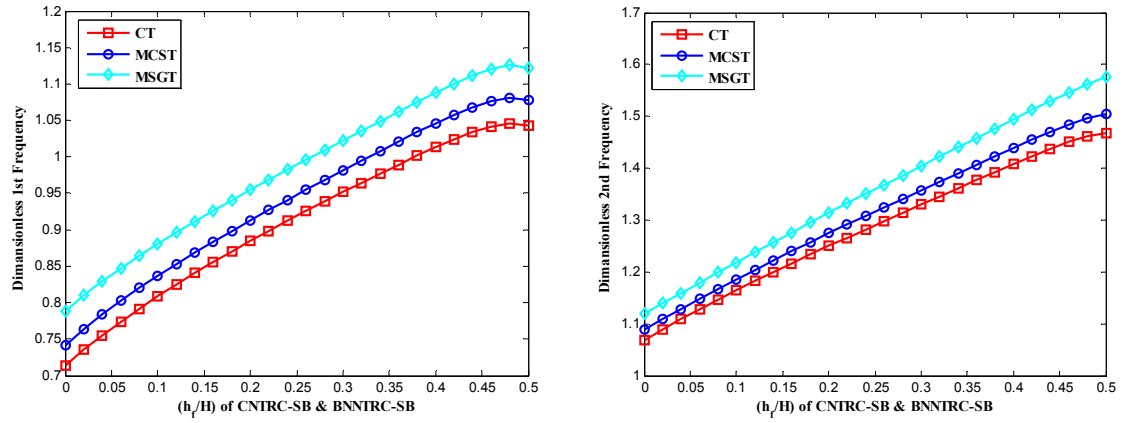

(a) (b)

Fig. 5 The effect of identical thickness ratio of two sandwich microbeams on the nonlinear frequency of double-bonded sandwich beams for various theories of size dependent effect: (a) 1st frequency; (b) 2nd frequency

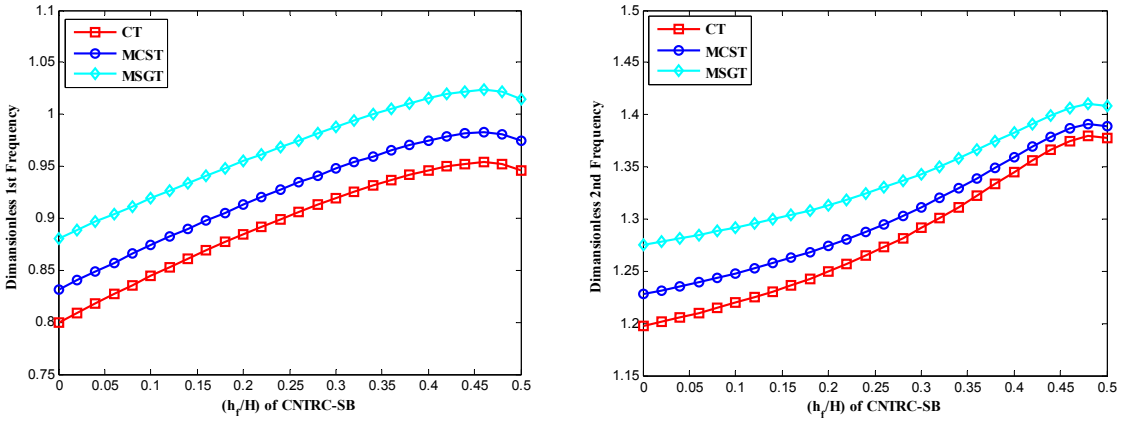

(a) (b)

Fig. 6 The effect of thickness ratio of CNTRC-SB on the nonlinear frequency of double-bonded sandwich microbeams for various theories of size dependent effect: (a) 1st frequency; (b) 2nd frequency

MSGT is higher than the other theories. It is due to that three material length scale parameters using MSGT leads to increase the stiffness of double-bonded sandwich Timoshenko beam.

The influence of electric and magnetic properties of BNNTRC and CNTRC on the first two dimensionless natural frequencies of double-bonded sandwich beams against slenderness ratio is depicted in Fig. 4. For given values in present work, it is obvious that although both electric and magnetic fields have low effect on the obtained results but the magnetic field of CNTRC has remarkable effect rather than electric field of BNNTRC.

The effect of identical thickness ratio of two sandwich beams ($(h_f/H)_{CNTRC\text{-}SB} = (h_f/H)_{BNNTRC\text{-}SB}$) on the first two dimensionless frequencies of double-bonded sandwich beams for various beam theories is represented in Fig. 5. As can be seen, the variation trend of dimensionless 1st frequency predicted by various types of size dependent effect is different with respect to dimensionless 2nd frequency. It is shown that with increasing thickness ratio of both sandwich beams, the 1st natural frequency increases firstly to achieve a maximum value for specific value of thickness ratio that approximately is equal to 0.48 and after this value, with an increase in the thickness ratio, 1st natural frequency decreases, whereas the variation of 2nd natural frequency is completely ascending for all values of thickness ratio. Moreover, it is found that with rising thickness ratio, the difference of 2nd natural frequency between various beam theories increases. It should be mentioned that when the thickness ratio of both sandwich beams are set to 0 ($(h_f/H)_{CNTRC\text{-}SB} = (h_f/H)_{BNNTRC\text{-}SB} = 0$), this means the case of double-bonded homogenous beams made of core material without considering face sheets and while this parameter is considered to 0.5 ($(h_f/H)_{CNTRC\text{-}SB} = (h_f/H)_{BNNTRC\text{-}SB} = 0.5$), the double-bonded sandwich beams convert to the double-bonded beams including CNTRC beam and BNNTRC beam without considering homogenous core.

Fig. 6 shows first two dimensionless natural frequencies of double-bonded sandwich beams for the different size dependent effect with the thickness ratio of CNTRC-SB beam. It is noted that the thickness ratio of BNNTRC-SB beam is constant in this figure. It is observed that the variation trend of dimensionless 1st and 2nd natural frequencies for various beam models is similar together where first, by enlarging CNTRC-SB thickness ratio, the 1st and 2nd natural frequencies increase until to yield its maximum value and then decrease. Also as depicted, the maximum value of 1st

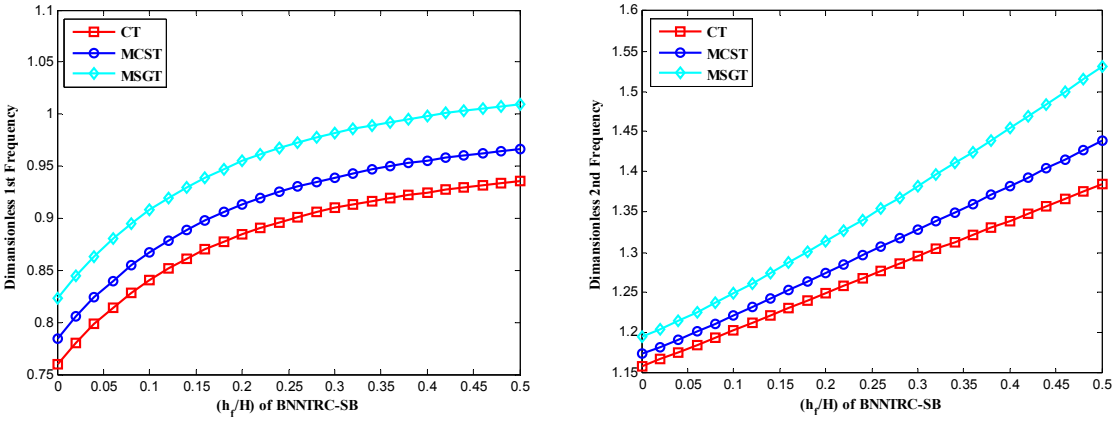

(a) (b)

Fig. 7 The effect of thickness ratio of BNNTRC-SB on the nonlinear frequency of double-bonded sandwich microbeams for various theories of size dependent effect: (a) 1st frequency; (b) 2nd frequency

and 2nd natural frequencies and associated stiffness for different beam models occur at thickness ratio of CNTRC-SB beam ($(h_f/H)_{CNTRC\text{-}SB}$) about 0.46 and 0.48, respectively.

Fig. 7 demonstrates the effect of thickness ratio of BNNTRC-SB beam on both the dimensionless 1st and 2nd natural frequencies of double-bonded sandwich beams using different size dependent theories. According to this figure, increasing the thickness ratio of BNNTRC-SB beam leads to higher values of dimensionless 1st and 2nd frequencies for various size dependent theories. It is noted that the thickness ratio of CNTRC-SB beam is constant in this figure. It can be seen that maximum frequency and associated stiffness can be obtained with thickness ratio equal to 0.5 ($(h_f/H)_{BNNTRC\text{-}SB}$ = 0.5). Also, the difference values of 2nd frequency between various beam models become larger when the thickness ratio increases. Furthermore, it is revealed that the

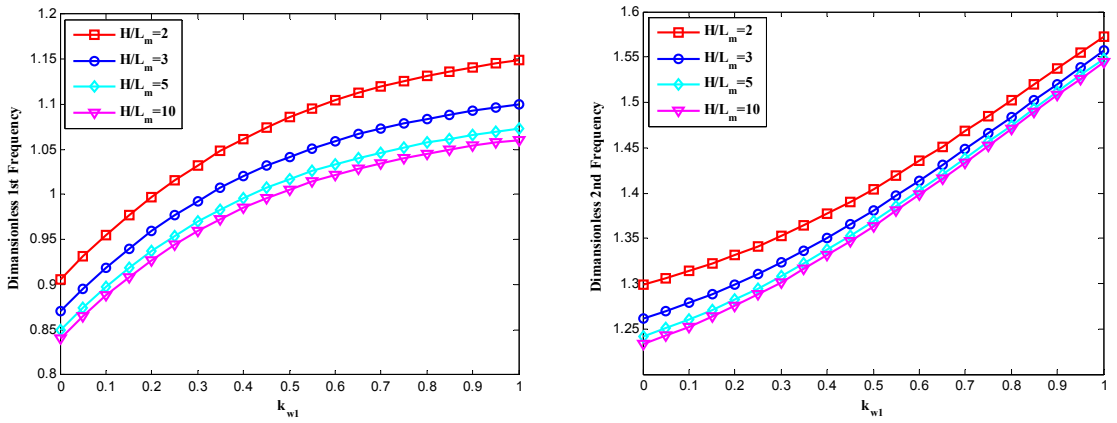

(a) (b)

Fig. 8 The effect of k_{w1} on the nonlinear frequency of double-bonded sandwich microbeams for strain gradient theory with different dimensionless material length scale parameter H/l_m: (a) 1st frequency; (b) 2nd frequency

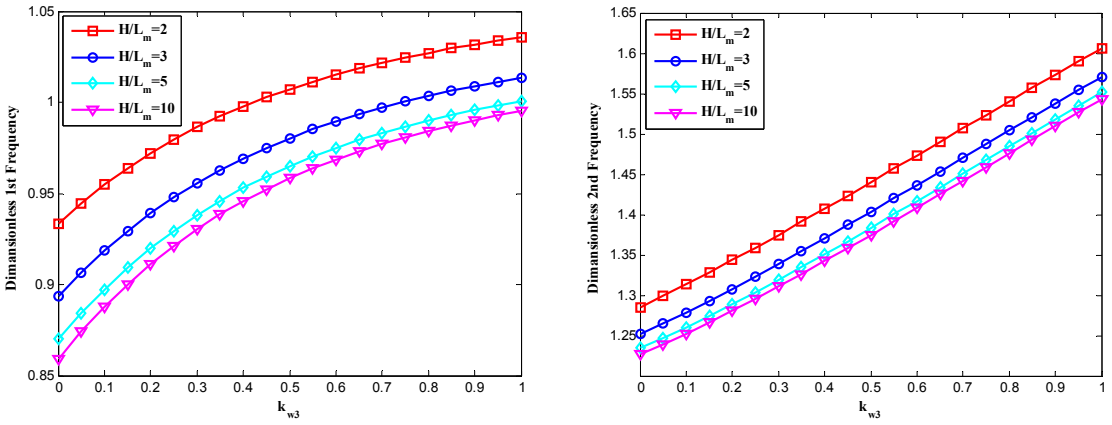

(a) (b)

Fig. 9 The effect of k_{w3} on the nonlinear frequency of double-bonded sandwich microbeams for strain gradient theory with different dimensionless material length scale parameter H/l_m: (a) 1st frequency; (b) 2nd frequency

increasing magnitude of 1st frequency for lower values of thickness ratio is more rate than that of 2nd frequency and this trend for higher values of thickness ratio become slight whereas this behavior for 2nd frequency is vice versa.

Fig. 8 shows the variation of dimensionless 1st and 2nd frequencies with the Winkler spring foundation no.1 (k_{w1}) calculated by MSGT beam model. It can be seen that by increasing the value of H/l_m, both the dimensionless 1st and 2nd frequencies decrease. Also, the concavity of curves for every frequency is contrary to other one or in other word, the concavity of 1st frequency curves is downward and negative whereas the concavity of 2nd frequency curves is upward and positive. In addition, it is clear that as the magnitude of k_{w1} increases, the obtained values of 1st frequency for different material length scale parameter have been diverged but the corresponding values of 2nd natural frequency have been converged.

The effect of Winkler spring foundation no. 3 (k_{w3}) on the dimensionless 1st and 2nd natural frequencies based on MSGT beam theory is indicated in Fig. 9. As illustrated in this figure, increasing in the Winkler spring modulus and dimensionless length scale parameter (H/l_m) leads to increase and decrease values of both the 1st and 2nd natural frequencies, respectively. It is found that the variation trend of dimensionless 1st frequency has been depicted as curves with negative concavity that the discrepancies between curves of H/l_m decrease slightly whereas the dimensionless 2nd frequency change linearly with respect to k_{w3} for different values of H/l_m and there is constant value of discrepancy between lines of H/l_m as k_{w3} value increases.

Figs. 10 and 11 show the variation of dimensionless 1st and 2nd natural frequencies of double-bonded sandwich beams versus Winkler spring modulus no. 1 (k_{w1}) and no. 3 (k_{w3}), respectively based on SGT with UD face sheets of CNTRC-SB and different distribution face sheets of BNNTRC-SB. As illustrated, for all cases, the FGA and FGV distribution types of BNNTRC-SB face sheets have the highest and lowest both the 1st and 2nd frequencies, respectively and for other them from up-to-down trend is followed by FGX, UD and FGO face sheets. It is revealed that the 1st natural frequency in both figures increases with enlarging the Winkler spring modulus, so that by decreasing k_{w1} and increasing k_{w3}, the 1st frequency for various cases of distribution are closed to each other and converged. For the dimensionless 2nd frequency, it can be seen that the

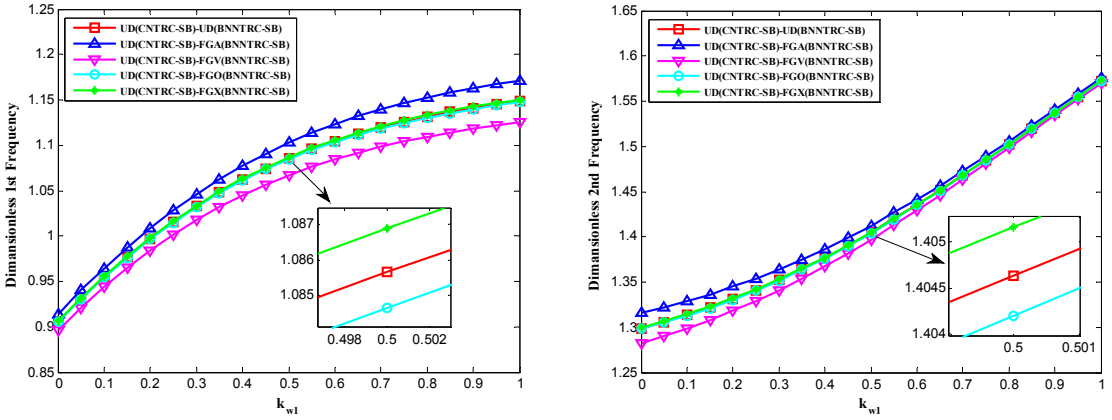

(a) (b)

Fig. 10 The effect of k_{w1} on the nonlinear frequency of double-bonded sandwich microbeams for strain gradient theory with UD face sheets of sandwich beam #1 and different face sheets of sandwich beam #2: (a) 1st frequency; (b) 2nd frequency

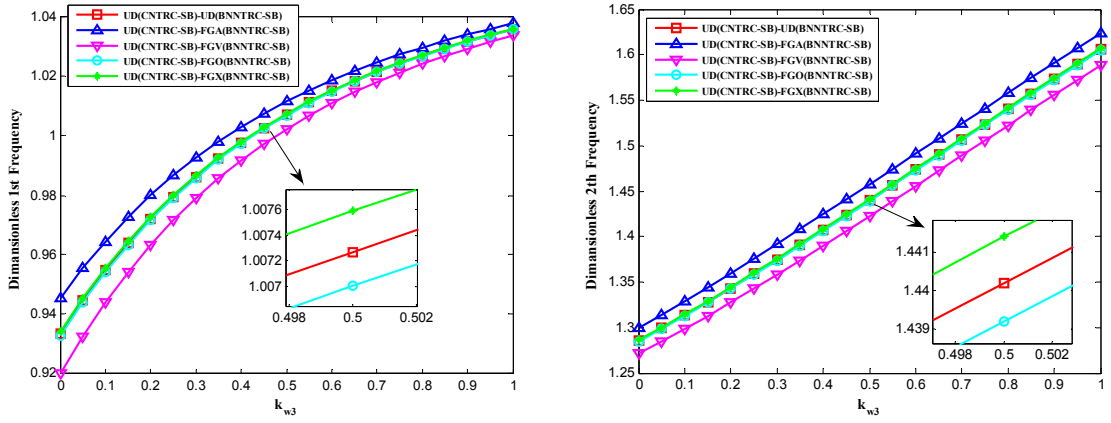

(a) (b)

Fig. 11 The effect of k_{w3} on the nonlinear frequency of double-bonded sandwich microbeams for strain gradient theory with UD face sheets of sandwich beam #1 and different face sheets of sandwich beam #2: (a) 1st frequency; (b) 2nd frequency

variation trend versus k_{w1} has been plotted as curves which by increasing the k_{w1} value, these curves for different distribution types tend to be converged but the behavior of 2nd frequency against k_{w3} is quite linearly that for all amount values of k_{w3}, the difference between various distribution types is a constant value. In other word, the distribution type of face sheet has more remarkable effect on the 1st frequency for lower values of k_{w3} and higher values of k_{w1}.

Figs. 12 and 13 represent the variation of dimensionless 1st and 2nd natural frequencies of double-bonded sandwich beams against Winkler spring modulus no. 1 (k_{w1}) and no. 3 (k_{w3}), respectively based on SGT with different distribution face sheets of CNTRC-SB and UD face

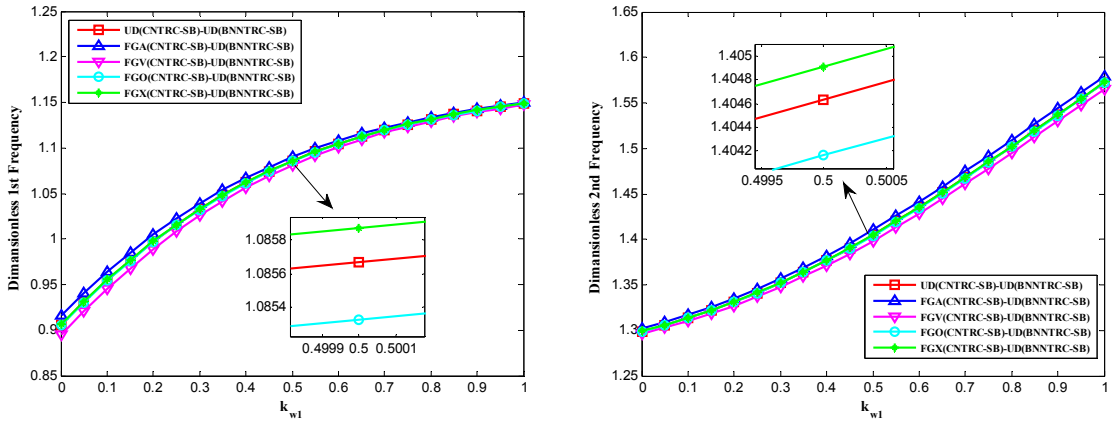

(a) (b)

Fig. 12 The effect of k_{w1} on the nonlinear frequency of double-bonded sandwich microbeams for strain gradient theory with different face sheets of sandwich beam #1 and UD face sheets of sandwich beam #2: (a) 1st frequency; (b) 2nd frequency

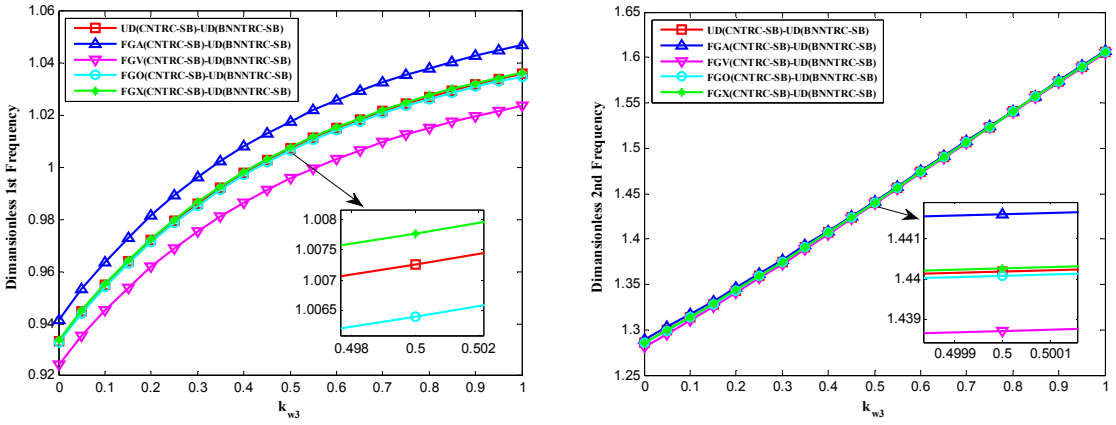

(a) (b)

Fig. 13 The effect of k_{w3} on the nonlinear frequency of double-bonded sandwich microbeams for strain gradient theory with different face sheets of sandwich beam #1 and UD face sheets of sandwich beam #2: (a) 1st frequency; (b) 2nd frequency

sheets of BNNTRC-SB. As plotted in these figures, the influence of k_{w3} value on the 1st frequency is more prominent for different distribution types rather than k_{w1} value so that for higher values of k_{w1} there is no noticeable difference amount between obtained 1st frequencies of various distribution types. Another point in this figure is that the 2nd frequency varies linearly respect to k_{w3} and the face sheet distribution type has not considerable effect. It is also found that the variation trend of 2nd frequency against k_{w1} and k_{w3} is curvature and linear, respectively where the effect of different distribution types of face sheets for varying k_{w3} value is negligible and also this behavior for higher values of k_{w1} is considerable than lower ones.

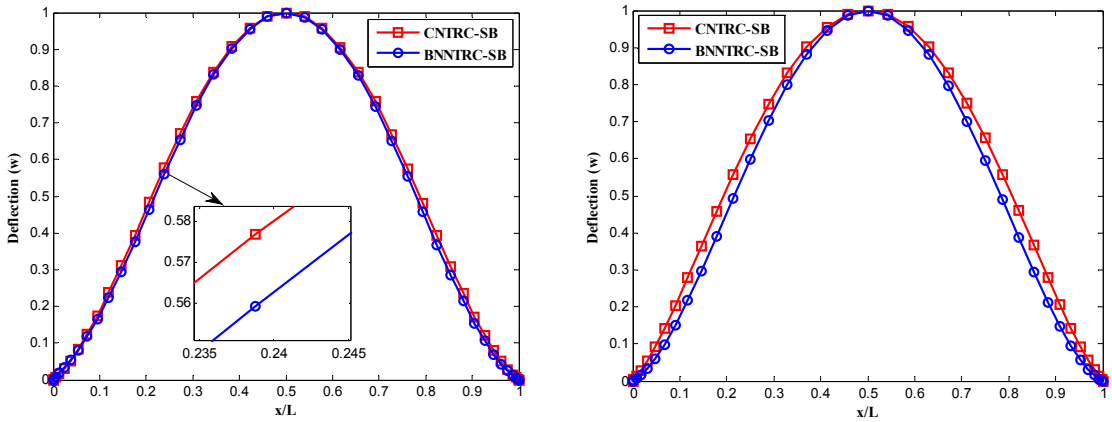

(a) (b)

Fig. 14 The nonlinear mode-shapes of deflection w for the both sandwich microbeams: (a) 1st frequency; (b) 2nd frequency

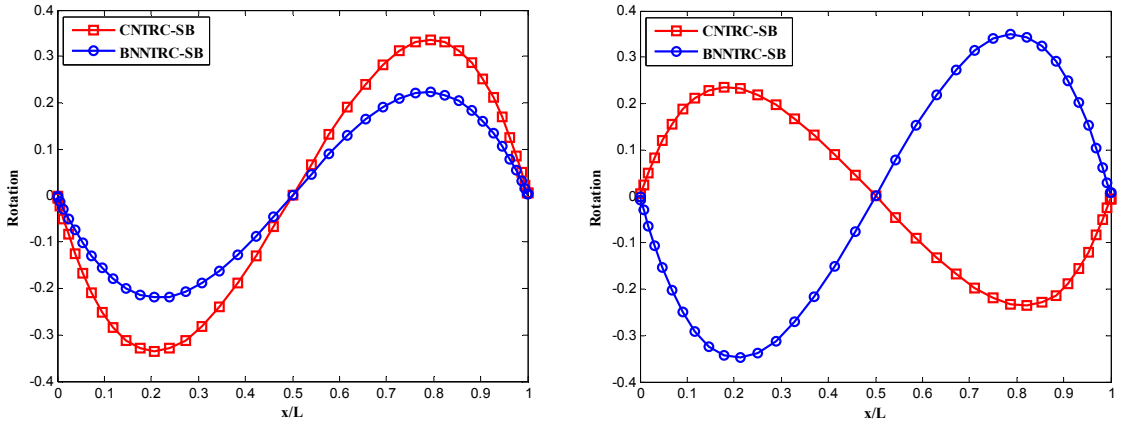

(a) (b)

Fig. 15 The nonlinear mode-shapes of rotation ψ for the both sandwich microbeams: (a) 1st frequency; (b) 2nd frequency

The nonlinear mode-shapes of the displacement (w) and rotation (ψ) for the lower (CNTRC-SB) and upper (BNNTRC-SB) sandwich microbeams corresponding to first two nonlinear natural frequencies are shown in Figs. 14 and 15, respectively.

From Fig. 14, it can be seen that the maximum amplitude of transverse vibration of each sandwich microbeam is located at the middle of it. Also, as plotted in Fig. 15, the 1st mode-shape of rotation behavior along the both lower and upper sandwich microbeams is similar together whereas this trend for 2nd mode shape of them is vice versa. On the other hand, the both sandwich microbeams for the 1st natural frequency rotate in the same direction but for the 2nd frequency have opposite rotation axis or 1st and 2nd natural frequencies are in-phase and out-phase, respectively.

6. Conclusions

In the present study, a magneto-electro-mechanical analysis of size-dependent double-bonded sandwich Timoshenko beams containing three additional material length scale parameters was developed based on MSGT. By using the Hamilton's principle, the non-classical governing equations of motion were derived. The current double-bonded sandwich Timoshenko beams formulation can be transformed to MSGT, MCST, and CT models for specific values of material length scale parameters. By employing GDQM, various numerical results were presented to indicate the influence of electric and magnetic fields, slenderness ratio, thickness ratio of both sandwich beams, thickness ratio of every sandwich beam, dimensionless length scale parameter, Winkler spring modulus and various distribution types of face sheets on the first two natural frequencies of double-bonded sandwich beams. It was yielded that the thickness ratios of sandwich beam play an important role in the vibration behavior of the double-bonded sandwich beams. The obtained main points from the results are as follows:

(1) It is revealed that although both electric and magnetic fields have low effect on the obtained results but the magnetic field of CNTRC has considerable effect rather than electric field of BNNTRC.
(2) Using various arrangements of Winkler spring constant, it is found that for different slenderness ratio, the value of k_{w1} has most influence on the 1st frequency in comparison to other Winkler springs, whereas the 2nd frequency has been highly affected with the k_{w2} value.
(3) Assuming geometrical and physical parameters in present work, the following cases have been investigated as:
    (a) With varying similar thickness ratio of both sandwich beams ($(h_f/H)_{CNTRC\text{-}SB} = (h_f/H)_{BNNTRC\text{-}SB}$), the maximum value of 1st and 2nd natural frequencies of double-bonded sandwich beams for different beam models occur at thickness ratios 0.48 and 0.50, respectively.
    (b) With varying thickness ratio of CNTRC-SB ($(h_f/H)_{CNTRC\text{-}SB}$), the maximum value of 1st and 2nd natural frequencies of double-bonded sandwich beams for different beam models occur at thickness ratio 0.46 and 0.48, respectively.
    (c) With varying thickness ratio of BNNTRC-SB ($(h_f/H)_{BNNTRC\text{-}SB}$), the maximum value of both 1st and 2nd natural frequencies of double-bonded sandwich beams for different beam models occur at thickness ratio 0.50.
(4) Increasing the value of H/l_m leads to decrease both 1st and 2nd natural frequencies. Moreover, as the magnitude of k_{w1} increases, the obtained values of 1st frequency for different material length scale parameter have been diverged but the corresponding values of 2nd natural frequency have been converged. In addition by increasing k_{w3}, the discrepancies between curves of H/l_m decrease slightly.
(5) Considering 1st natural frequency, the distribution type of BNNTRC-SB face sheets has more remarkable effect for lower values of k_{w3} and higher values of k_{w1} whereas for various distribution types of CNTRC-SB face sheets, the influence of k_{w3} value is more prominent rather than k_{w1} value.
(6) By increasing the value of k_{w1}, the obtained 2nd natural frequency for different distribution types of BNNTRC-SB face sheets tends to be converged and its behavior against k_{w3} is quite linearly, whereas the effect of different distribution types of CNTRC-SB face sheets

for varying k_{w1} value is negligible and also this behavior for higher values of k_{w3} is considerable than lower ones.

Acknowledgments

The authors would like to thank the referees for their valuable comments. They are also grateful to the Iranian Nanotechnology Development Committee for their financial support and the University of Kashan for supporting this work by Grant No. 463855/9.

References

Akgöz, B. and Civalek, Ö. (2011), "Strain gradient elasticity and modified couple stress models for buckling analysis of axially loaded micro-scaled beams", *Int. J. Eng. Sci.*, **49**(11), 1268-1280.

Akgöz, B. and Civalek, Ö. (2012), "Analysis of micro-sized beams for various boundary conditions based on the strain gradient elasticity theory", *Arch. Appl. Mech.*, **82**(3), 423-443.

Akgöz, B. and Civalek, Ö. (2013a), "Buckling analysis of functionally graded microbeams based on the strain gradient theory", *Acta. Mech.*, **224**(9), 1-17.

Akgöz, B. and Civalek, Ö. (2013b), "A size-dependent shear deformation beam model based on the strain gradient elasticity theory", *Int. J. Eng. Sci.*, **70**, 1-14.

Alibeigloo, A. and Liew, K.M. (2014), "Free vibration analysis of sandwich cylindrical panel with functionally graded core using three-dimensional theory of elasticity", *Compos. Struct.*, **113**, 23-30.

Allen, H.G. (1969), *Analysis and Design of Structural Sandwich Panels*, Pergamon Press, London, UK

Ansari, R., Gholami, R. and Sahmani, S. (2011), "Free vibration analysis of size-dependent functionally graded microbeams based on the strain gradient Timoshenko beam theory", *Compos. Struct.*, **94**(1), 221-228.

Ansari, R., Gholami, R., Faghih Shojaei, M., Mohammadi, V. and Sahmani, S. (2013), "Size-dependent bending, buckling and free vibration of functionally graded Timoshenko microbeams based on the most general strain gradient theory", *Compos. Struct.*, **100**, 385-397.

Bourada, M., Kaci, A., Houari, M.S.A. and Tounsi, A. (2015), "A new simple shear and normal deformations theory for functionally graded beams", *Steel Compos. Struct., Int. J.*, **18**(2), 409-423.

Bouremana, M., Houari, M.S.A., Tounsi, A., Kaci, A. and Bedia, E.A.A. (2013), "A new first shear deformation beam theory based on neutral surface position for functionally graded beams", *Steel Compos. Struct., Int. J.*, **15**(5), 467-479.

Bui, T.Q., Khosravifard, A., Zhang, C., Hematiyan, M.R. and Golub, M.V. (2013), "Dynamic analysis of sandwich beams with functionally graded core using a truly meshfree radial point interpolation method", *Eng. Struct.*, **47**, 90-104.

Chehel Amirani, M., Khalili, S.M.R. and Nemati, N. (2009), "Free vibration analysis of sandwich beam with FG core using the element free Galerkin method", *Compos. Struct.*, **90**(3), 373-379.

Damanpack, A.R. and Khalili, S.M.R. (2012), "High-order free vibration analysis of sandwich beams with a flexible core using dynamic stiffness method", *Compos. Struct* , **94**(5), 1503-1514.

Dariushi, S. and Sadighi, M. (2013), "A new nonlinear high order theory for sandwich beams: An analytical and experimental investigation", *Compos. Struct.*, **108**, 779-788.

Fleck, N.A. and Hutchinson, J.W. (1993), "A phenomenological theory for strain gradient effects in plasticity", *J. Mech. Phys. Solids.*, **41**(12), 1825-1857.

Ghasemi, H., Brighenti, R., Zhuang, X., Muthu, J. and Rabczuk, T. (2014a), "Optimization of fiber distribution in fiber reinforced composite by using NURBS functions", *Comput. Mater. Sci.*, **83**(15), 463-473.

Ghasemi, H., Rafiee, R., Zhuang, X., Muthu, J., Rabczuk, T. (2014b), "Uncertainties propagation in metamodel-based probabilistic optimization of CNT/polymer composite structure using stochastic multi-scale modeling", *Comput. Mater. Science*, **85**, 295-305.

Ghasemi, H., Kerfriden, P., Bordas, S.P.A., Muthu, J., Zi, G. and Rabczuk, T. (2014c), "Interfacial shear stress optimization in sandwich beams with polymeric core using non-uniform distribution of reinforcing ingredients", *Compos. Struct.*, **120**, 221-230.

Ghasemi, H., Brighenti, R., Zhuang, X., Muthu, J. and Rabczuk, T. (2015), "Optimal fiber content and distribution in fiber-reinforced solids using a reliability and NURBS based sequential optimization approach", *Struct. Multidisc. Optim.*, **51**(1), 99-112.

Ghorbanpour Arani, A. and Amir, S. (2013), "Electro-thermal vibration of visco-elastically coupled BNNT systems conveying fluid embedded on elastic foundation via strain gradient theory", *Physica B*, **419**, 1-6.

Ghorbanpour Arani, A., Haghparast, E., Heidari Rarani, M. and Khoddami Maraghi, Z. (2015), "Strain gradient shell model for nonlinear vibration analysis of visco-elastically coupled Boron Nitride nano-tube reinforced composite micro-tubes conveying viscous fluid", *Comput. Mater. Sci.*, **96**, 448-458.

Griebel, M. and Hamaekers, J. (2004), "Molecular dynamics simulations of the elastic moduli of polymer–carbon nanotube composites", *Comput. Meth. Appl. Mech. Eng.*, **193**, 1773-1788.

Grygorowicz, M., Magnucki, K. and Malinowski, M. (2015), "Elastic buckling of a sandwich beam with variable mechanical properties of the core", *Thin-Walled Struct.*, **87**, 127-132.

Han, Y. and Elliott, J. (2007), "Molecular dynamics simulations of the elastic properties of polymer/carbon nanotube composites", *Comput. Mater. Sci.*, **39**(2), 315-323.

Jedari Salami, S., Sadighi, M. and Shakeri, M. (2015), "Improved High order analysis of sandwich beams by considering a bilinear elasto-plastic behavior of core: An analytical and experimental investigation", *Int. J. Mech. Sci.*, **93**, 270-289.

Kahrobaiyan, M.H., Rahaeifard, M., Tajalli, S.A. and Ahmadian, MT. (2012), "A strain gradient functionally graded Euler–Bernoulli beam formulation", *Int. J. Eng. Sci.*, **52**, 65-76.

Kong, S., Zhou, S., Nie, Z. and Wang, K. (2009), "Static and dynamic analysis of microbeams based on strain gradient elasticity theory", *Int. J. Eng. Sci.*, **47**(4), 487-498.

Lam, D.C.C., Yang, F., Chong, A.C.M., Wang, J. and Tong, P. (2003), "Experiments and theory in strain gradient elasticity", *J. Mech. Phys. Solids*, **51**(8), 1477-1508.

Lanc, D., Vo, T.P., Turkalj, G. and Lee, J. (2015), "Buckling analysis of thin-walled functionally graded sandwich box beams", *Thin-Wall. Struct.*, **86**, 148-156.

Lei, J., He, Y., Zhang, B., Gan, Z. and Zeng, P. (2013), "Bending and vibration of functionally graded sinusoidal microbeams based on the strain gradient elasticity theory", *Int. J. Eng. Sci.*, **72**, 36-52.

Liang, X., Hu, S. and Shen, S. (2014), "A new Bernoulli-Euler beam model based on a simplified strain gradient elasticity theory and its applications", *Compos. Struct.*, **111**, 317-323.

Liew, K.M., Lei, Z.X. and Zhang, L.W. (2015), "Mechanical analysis of functionally graded carbon nanotube reinforced composites: A review", *Compos. Struct.*, **120**, 90-97.

Mohammadimehr, M., Saidi, A.R., Ghorbanpour Arani, A., Arefmanesh, A. and Han, Q. (2010), "Torsional buckling of a DWCNT embedded on winkler and pasternak foundations using nonlocal theory", *J. Mech. Sci. Technol.*, **24**(6), 1289-1299.

Mohammadimehr, M., Monajemi, A.A. and Moradi, M. (2015a), "Vibration analysis of viscoelastic tapered micro-rod based on strain gradient theory resting on visco-pasternak foundation using DQM", *J. Mech. Sci. Technol.*, **29**(6), 2297-2305.

Mohammadimehr, M., Rousta Navi, B. and Ghorbanpour Arani, A. (2015b), "Free vibration of viscoelastic double-bonded polymeric nanocomposite plates reinforced by FG-SWCNTs using MSGT, sinusoidal shear deformation theory and meshless method", *Compos. Struct.*, **131**, 654-671.

Mohammadimehr, M., Rostami, R. and Arefi, M. (2016a), "Electro-elastic analysis of a sandwich thick plate considering FG core and composite piezoelectric layers on Pasternak foundation using TSDT", *Steel Compos. Struct., Int. J.*, **20**(3), 513-543.

Mohammadimehr, M., Rousta Navi, B. and Ghorbanpour Arani, A. (2016b), "Modified strain gradient Reddy rectangular plate model for biaxial buckling and bending analysis of double-coupled piezoelectric

polymeric nanocomposite reinforced by FG-SWNT", *Compos. Part B*, **87**, 132-148.
Mohammadimehr, M., Salemi, M. and Rousta Navi, B. (2016c), "Bending, buckling, and free vibration analysis of MSGT microcomposite Reddy plate reinforced by FG-SWCNTs with temperature- dependent material properties under hydro-thermo-mechanical loadings using DQM", *Compos. Struct.*, **138**, 361-380.
Nanthakumar, S., Valizadeh, N., Park, H.S. and Rabczuk, T. (2015), "Shape and topology optimization of nanostructures using a coupled XFEM/level set method", *Comput. Mech.*, **56**(1), 97-112.
Plantema, F.J. (1966), *Sandwich Construction: The Bending and Buckling of Sandwich Beams*, *Plates and Shells*, John Wiley and Sons, New York, NY, USA.
Rahmani, O., Khalili, S.M.R., Malekzadeh, K. and Hadavinia, H. (2009), "Free vibration analysis of sandwich structures with a flexible functionally graded syntactic core", *Compos. Struct.*, **91**(2), 229-235.
Reissner, E. (1948), "Finite deflections of sandwich plates", *J. Aeronaut. Sci.*, **15**(7), 435-440.
Sahmani, S. Bahrami, M. and Ansari, R. (2014), "Nonlinear free vibration analysis of functionally graded third-order shear deformable microbeams based on the modified strain gradient elasticity theory", *Compos. Struct.*, **110**, 219-230.
Salehi-Khojin, A. and Jalili, N. (2008), "Buckling of boron nitride nanotube reinforced piezoelectric polymeric composites subject to combined electro-thermo-mechanical loadings", *Compos. Sci. Technol.*, **68**(6), 1489-1501.
Shu, C. (2000), *Differential Quadrature and its Application in Engineering*, Springer Publication, New York, NY, USA.
Shu, C. and Du, H. (1997), "Implementation of clamped and simply supported boundary conditions in the GDQ free vibration analysis of beams and plates", *J. Sound Vib.*, **34**(7), 819-835.
Taibi, F.Z., Benyoucef, S., Tounsi, A., Bouiadjra, R.B., Bedia, A.A. and Mahmoud, S. (2015), "A simple shear deformation theory for thermo-mechanical behaviour of functionally graded sandwich plates on elastic foundations", *J. Sandw. Struct. Mater.*, **17**, 99-129.
Tajalli, S.A., Rahaeifard, M., Kahrobaiyan, M.H., Movahhedy, M.R., Akbari, J. and Ahmadian, M.T. (2013), "Mechanical behavior analysis of size-dependent micro-scaled functionally graded Timoshenko beams by strain gradient elasticity theory", *Compos. Struct.*, **102**, 72-80.
Vinson, J.R. (1999), *The Behavior of Sandwich Structures of Isotropic and Composite Materials*, Technomic Publishing Co. Inc., Lancaster, England.
Vo, T.P., Thai, H.T., Nguyen, T.K., Maheri, A. and Lee, J. (2014), "Finite element model for vibration and buckling of functionally graded sandwich beams based on a refined shear deformation theory", *Eng. Struct.*, **64**, 12-22.
Vo, T.P., Thai, H.T., Nguyen, T.K., Inam, F. and Lee, J. (2015), "A quasi-3D theory for vibration and buckling of functionally graded sandwich beams", *Compos. Struct.*, **119**, 1-12.
Wang, Z.X. and Shen, H.S. (2011), "Nonlinear analysis of sandwich plates with FGM face sheets resting on elastic foundations", *Compos. Struct.*, **93**(10), 2521-2532.
Wang, Z.X. and Shen, H.S. (2012), "Nonlinear vibration and bending of sandwich plates with nanotube-reinforced composite face sheets", *Compos. Part B*, **43**(2), 411-421.
Wang, Y. and Wang, X. (2014), "Static analysis of higher order sandwich beams by weak form quadrature element method", *Compos. Struct.*, **116**, 841-848.
Wang, B., Zhao, J. and Zhou, S. (2010), "A microscale Timoshenko beam model based on strain gradient elasticity theory", *Eur. J. Mech. A-Solid*, **29**(4), 591-599.
Yang, F., Chong, A.C.M. and Lam, D.C.C. (2002), "Couple stress based strain gradient theory for elasticity", *Int. J. Solid. Struct.*, **39**(10), 2731-2743.
Yang, Y., Lam, C.C., Kou, K.P. and Iu, V.P. (2014), "Free vibration analysis of the functionally graded sandwich beams by a meshfree boundary-domain integral equation method", *Compos. Struct.*, **117**, 32-39.
Yas, M.H. and Samadi, N. (2012), "Free vibrations and buckling analysis of carbon nanotube-reinforced composite Timoshenko beams on elastic foundation", *Int. J. Pressure Vessels Pip.*, **98**, 119-128.
Zenkert, D. (1995), *An Introduction to Sandwich Construction*, Chameleon Press Ltd., London, UK.
Zhang, C.L. and Shen, H.S. (2006), "Temperature-dependent elastic properties of single-walled carbon nanotubes: prediction from molecular dynamics simulation", *Appl. Phys. Lett.*, **89**(8), 081904.

Zhang, B., He, Y., Liu, D., Gan, Z. and Shen, L. (2014), "Non-classical Timoshenko beam element based on the strain gradient elasticity theory", *Finite Elem. Anal. Des.*, **79**, 22-39.

CC

Nomenclature

A	cross-sectional area of sandwich beam
BNNT	Boron nitride nanotube
BNNTRC	Boron nitride nanotube reinforced composite
BNNTRC-SB	Sandwich beam with boron nitride nanotube reinforced composite face sheets
CNT	Carbon nanotube
CNTRC	Carbon nanotube reinforced composite
CNTRC-SB	Sandwich beam with carbon nanotube reinforced composite face sheets
CT	Classical theory
DQM	Differential quadrature method
FG	Functionally graded
FG-BNNTRC	Functionally graded boron nitride nanotube reinforced composite
FG-CNTRC	Functionally graded carbon nanotube reinforced composite
GDQM	Generalized differential quadrature method
H	Total thickness of sandwich beam
L	Length of sandwich beam
MCST	Modified couple stress theory
MD	Molecular dynamics
MSGT	Modified strain gradient theory
PMMA	Poly methyl methacrylate
PVDF	Poly vinylidene fluoride
SGT	Strain gradient theory
UD	Uniform distribution
U_1, U_2, U_3	x, y and z components of displacement vector
w_{RC}	Mass fraction of BNNT or CNT
k_s	Shear correction factor
h_f^C , h_c^C	Thicknesses of face sheet and core of CNTRC-SB, respectively
h_f^B , h_c^B	Thicknesses of face sheet and core of BNNTRC-SB, respectively
ρ_c, ρ_{cnt}^C, ρ_m^C	Density of the core, carbon nanotube and matrix of CNTRC-SB, respectively

$\upsilon_c, \upsilon_{cnt}^C, \upsilon_m^C$	Poisson's ratio of the core, carbon nanotube and matrix of CNTRC-SB, respectively
$E_c, E_{11}^{cnt}, E_{22}^{cnt}, E_m^C$	Young's modulus of core, carbon nanotube and matrix of CNTRC-SB, respectively
G_c, G_{12}^{cnt}, G_m^C	Shear modulus of core, carbon nanotube and matrix of CNTRC-SB, respectively
η_1, η_2, η_3	Efficiency parameters of carbon nanotube
V_{cnt}, V_{bnnt}, V_m	Volume fractions of CNT, BNNT and matrix, respectively
$\alpha_{cnt}^C, \alpha_m^C, \alpha_{bnnt}^B, \alpha_m^B$	Thermal expansion coefficient of CNT, PMMA, BNNT, PVDF, respectively
$\varepsilon_{xx}, \gamma_{xz}$	Normal and shear strain, respectively
$\delta V, \delta W, \delta T$	Virtual strain energy, virtual work done by external forces, virtual kinetic energy, respectively

Appendix A

By inserting Eqs. (14) and (15) into Eq. (11), the following nonzero components of γ, χ^s and $\eta^{(1)}$ that are defined as the following form

$$\begin{aligned}
&\gamma_x = \frac{\partial^2 U}{\partial x^2} + z\frac{\partial^2 \Psi}{\partial x^2} + \frac{\partial W}{\partial x}\frac{\partial^2 W}{\partial x^2}, \quad \gamma_Z = \frac{\partial \Psi}{\partial x} \\
&\chi_{xy}^S = \chi_{yx}^S = \frac{1}{8}\left(-\frac{\partial^2 W}{\partial x^2} + \frac{\partial \Psi}{\partial x}\right) \\
&\eta_{xxx}^{(1)} = \frac{2}{5}\left(\frac{\partial^2 U}{\partial x^2} + z\frac{\partial^2 \Psi}{\partial x^2} + \frac{\partial W}{\partial x}\frac{\partial^2 W}{\partial x^2}\right) \\
&\eta_{zzz}^{(1)} = -\frac{1}{5}\left(\frac{\partial^2 W}{\partial x^2} + 2\frac{\partial \Psi}{\partial x}\right) \\
&\eta_{xxz}^{(1)} = \eta_{xzx}^{(1)} = \eta_{zxx}^{(1)} = \frac{4}{15}\left(\frac{\partial^2 W}{\partial x^2} + 2\frac{\partial \Psi}{\partial x}\right) \\
&\eta_{yyz}^{(1)} = \eta_{yzy}^{(1)} = \eta_{zyy}^{(1)} = -\frac{1}{15}\left(\frac{\partial^2 W}{\partial x^2} + 2\frac{\partial \Psi}{\partial x}\right) \\
&\eta_{xyy}^{(1)} = \eta_{yxy}^{(1)} = \eta_{yyx}^{(1)} = \eta_{xzz}^{(1)} = \eta_{zxz}^{(1)} = \eta_{zzx}^{(1)} = -\frac{1}{5}\left(\frac{\partial^2 U}{\partial x^2} + z\frac{\partial^2 \Psi}{\partial x^2} + \frac{\partial W}{\partial x}\frac{\partial^2 W}{\partial x^2}\right)
\end{aligned} \tag{A-1}$$

Also, the nonzero components of the classical stress tensor are expressed as follows:

$$\begin{aligned}
&\sigma_{xx}^C = Q_{11}\left[\frac{\partial U}{\partial x} + z\frac{\partial \Psi}{\partial x} + \frac{1}{2}\left(\frac{\partial W}{\partial x}\right)^2 - \alpha_T^C.\Delta T\right] + q_{11}\Omega_{,x} \\
&\sigma_{xx}^B = Q_{11}\left[\frac{\partial U}{\partial x} + z\frac{\partial \Psi}{\partial x} + \frac{1}{2}(\ )^2 - \alpha_T^B.\Delta T\right] + h_{11}\Omega_{,x} \\
&\tau_{xz} = k_s Q_{55}\left(\frac{\partial W}{\partial x} + \Psi\right)
\end{aligned} \tag{A-2}$$

The correction shear factor k_s, which is depends on the shape of cross-section of beam, is multiplied into the shear stress τ_{xz} to take the non-uniformity of the shear strain into account over the beam cross-section.

Appendix B

By substituting Eqs. (A-1) and (A-2) into Eq. (12), the nonzero components of the higher-order stresses can be obtained follows

$$p_x = 2Gl_0^2\left(\frac{\partial^2 U}{\partial x^2} + z\frac{\partial^2 \Psi}{\partial x^2} + \frac{\partial W}{\partial x}\frac{\partial^2 W}{\partial x^2}\right), \quad p_z = 2Gl_0^2\frac{\partial \Psi}{\partial x} \tag{B-1}$$

$$m_{xy}^s = m_{yx}^s = \frac{1}{4}Gl_2^2\left(\frac{\partial \Psi}{\partial x} - \frac{\partial^2 W}{\partial x^2}\right) \tag{B-2}$$

$$\begin{aligned}
&\tau_{xxx}^{(1)} = \frac{4}{5}Gl_1^2\left(\frac{\partial^2 U}{\partial x^2} + z\frac{\partial^2 \Psi}{\partial x^2} + \frac{\partial W}{\partial x}\frac{\partial^2 W}{\partial x^2}\right)\\
&\tau_{zzz}^{(1)} = -\frac{2}{5}Gl_1^2\left(\frac{\partial^2 W}{\partial x^2} + 2\frac{\partial \Psi}{\partial x}\right)\\
&\tau_{xxz}^{(1)} = \tau_{xzx}^{(1)} = \tau_{zxx}^{(1)} = \frac{8}{15}Gl_1^2\left(\frac{\partial^2 W}{\partial x^2} + 2\frac{\partial \Psi}{\partial x}\right)\\
&\tau_{yyz}^{(1)} = \tau_{yzy}^{(1)} = \tau_{zyy}^{(1)} = -\frac{2}{15}Gl_1^2\left(\frac{\partial^2 W}{\partial x^2} + 2\frac{\partial \Psi}{\partial x}\right)\\
&\tau_{xyy}^{(1)} = \tau_{yxy}^{(1)} = \tau_{yyx}^{(1)} = \tau_{xzz}^{(1)} = \tau_{zxz}^{(1)} = \tau_{zzx}^{(1)} = -\frac{2}{5}Gl_1^2\left(\frac{\partial^2 U}{\partial x^2} + z\frac{\partial^2 \Psi}{\partial x^2} + \frac{\partial W}{\partial x}\frac{\partial^2 W}{\partial x^2}\right)
\end{aligned} \tag{B-3}$$

Appendix C

Taking the variation of U_1, W_1, Ψ_1 and Ω_1 for CNTRC-SB and U_2, W_2, Ψ_2 and Φ_2 for BNNTRC-SB by using Eqs. (17)-(21) and according to Eq. (16), the governing equations of motion for both sandwich beams using the clamped-clamped boundary conditions are obtained as follows

For CNTRC-SB:

$$
\begin{aligned}
&\delta U_1: \\
&-A_{11C}\left(\frac{\partial^2 U_1}{\partial x^2}+\frac{\partial W_1}{\partial x}\frac{\partial^2 W_1}{\partial x^2}\right)+K_1A_{55C}\left(\frac{\partial^4 U_1}{\partial x^4}+3\frac{\partial^2 W_1}{\partial x^2}\frac{\partial^3 W_1}{\partial x^3}+\frac{\partial W_1}{\partial x}\frac{\partial^4 W_1}{\partial x^4}\right) \\
&-B_{11C}\frac{\partial^2 \Psi_1}{\partial x^2}+K_1B_{55C}\frac{\partial^4 \Psi_1}{\partial x^4}-2q_{11}h_f^C\frac{\partial^2 \Omega_1}{\partial x^2}+I_{0C}\frac{\partial^2 U_1}{\partial t^2}+I_{1C}\frac{\partial^2 \Psi_1}{\partial t^2}=0
\end{aligned}
$$

$$
\begin{aligned}
&\delta W_1: \\
&-A_{11C}\left(\frac{3}{2}\frac{\partial^2 W_1}{\partial x^2}\left(\frac{\partial W_1}{\partial x}\right)^2+\frac{\partial^2 U_1}{\partial x^2}\frac{\partial W_1}{\partial x}+\frac{\partial U_1}{\partial x}\frac{\partial^2 W_1}{\partial x^2}-\frac{\alpha_T^C.\Delta T}{2}\frac{\partial^2 W_1}{\partial x^2}\right) \\
&-B_{11C}\left(\frac{\partial W_1}{\partial x}\frac{\partial^2 \Psi_1}{\partial x^2}+\frac{\partial^2 W_1}{\partial x^2}\frac{\partial \Psi_1}{\partial x}\right)-k_sA_{55C}\left(\frac{\partial^2 W_1}{\partial x^2}+\frac{\partial \Psi_1}{\partial x}\right) \\
&-2q_{11}h_f^C\left(\frac{\partial \Omega_1}{\partial x}\frac{\partial^2 W_1}{\partial x^2}+\frac{\partial^2 \Omega_1}{\partial x^2}\frac{\partial W_1}{\partial x}\right) \\
&+K_1A_{55C}\left(\begin{array}{l}\left(\frac{\partial^2 W_1}{\partial x^2}\right)^3+4\frac{\partial W_1}{\partial x}\frac{\partial^2 W_1}{\partial x^2}\frac{\partial^3 W_1}{\partial x^3}+\left(\frac{\partial W_1}{\partial x}\right)^2\frac{\partial^4 W_1}{\partial x^4} \\ +2\frac{\partial^2 U_1}{\partial x^2}\frac{\partial^3 W_1}{\partial x^3}+3\frac{\partial^3 U_1}{\partial x^3}\frac{\partial^2 W_1}{\partial x^2}+\frac{\partial^4 U_1}{\partial x^4}\frac{\partial W_1}{\partial x}\end{array}\right) \\
&+K_1B_{55C}\left(\frac{\partial W_1}{\partial x}\frac{\partial^4 \Psi_1}{\partial x^4}+\frac{\partial^2 W_1}{\partial x^2}\frac{\partial^3 \Psi_1}{\partial x^3}\right)+K_2A_{55C}\left(\frac{\partial^4 W_1}{\partial x^4}+2\frac{\partial^3 \Psi_1}{\partial x^3}\right)+K_3A_{55C}\left(\frac{\partial^4 W_1}{\partial x^4}-\frac{\partial^3 \Psi_1}{\partial x^3}\right) \\
&+k_{w1}W_1-G_{p1}\frac{\partial^2 W_1}{\partial x^2}+k_{w2}\left(W_1-W_2\right)-G_{p2}\left(\frac{\partial^2 W_1}{\partial x^2}-\frac{\partial^2 W_2}{\partial x^2}\right)+I_{0C}\frac{\partial^2 W_1}{\partial t^2}-0
\end{aligned}
\tag{C-1}
$$

$\delta \Psi_1$:

$$
\begin{aligned}
&- D_{11C}\frac{\partial^2 \Psi_1}{\partial x^2} - B_{11C}\left(\frac{\partial^2 U_1}{\partial x^2} + \frac{\partial W_1}{\partial x}\frac{\partial^2 W_1}{\partial x^2}\right) - k_s A_{55C}\left(\frac{\partial W_1}{\partial x} + \Psi_1\right) \\
&+ K_1 B_{55C}\left(\frac{\partial^4 U_1}{\partial x^4} + 3\frac{\partial^2 W_1}{\partial x^2}\frac{\partial^3 W_1}{\partial x^3} + \frac{\partial W_1}{\partial x}\frac{\partial^4 W_1}{\partial x^4}\right) + K_1 D_{55C}\frac{\partial^4 \Psi_1}{\partial x^4} \\
&- K_2 A_{55C}\left(2\frac{\partial^3 W_1}{\partial x^3} + 4\frac{\partial^2 \Psi_1}{\partial x^2}\right) + K_3 A_{55C}\left(\frac{\partial^3 W_1}{\partial x^3} - \frac{\partial^2 \Psi_1}{\partial x^2}\right) + I_{2C}\frac{\partial^2 \Psi_1}{\partial t^2} + I_{1C}\frac{\partial^2 U_1}{\partial t^2} - 0
\end{aligned}
\tag{C-1}
$$

$\delta \Omega_1$:

$$
- q_{11} h_f^C \left(\frac{\partial^2 U_1}{\partial x^2} + 2\frac{\partial^2 W_1}{\partial x^2}\frac{\partial W_1}{\partial x}\right) + 2\mu_{11} h_f^C \Omega_{1,x} - 0
$$

For BNNTRC-SB:

δU_2 :

$$
\begin{aligned}
&- A_{11B}\left(\frac{\partial^2 U_2}{\partial x^2} + \frac{\partial W_2}{\partial x}\frac{\partial^2 W_2}{\partial x^2}\right) + K_1 A_{55B}\left(\frac{\partial^4 U_2}{\partial x^4} + 3\frac{\partial^2 W_2}{\partial x^2}\frac{\partial^3 W_2}{\partial x^3} + \frac{\partial W_2}{\partial x}\frac{\partial^4 W_2}{\partial x^4}\right) \\
&- B_{11B}\frac{\partial^2 \Psi_2}{\partial x^2} + K_1 B_{55B}\frac{\partial^4 \Psi_2}{\partial x^4} - 2h_{11} h_f^B \frac{\partial^2 \phi_2}{\partial x^2} + I_{0B}\frac{\partial^2 U_2}{\partial t^2} + I_{1B}\frac{\partial^2 \Psi_2}{\partial t^2} - 0
\end{aligned}
\tag{C-2}
$$

δW_2 :

$$
\begin{aligned}
&-A_{11B}\left(\frac{3}{2}\frac{\partial^2 W_2}{\partial x^2}\left(\frac{\partial W_2}{\partial x}\right)^2+\frac{\partial^2 U_2}{\partial x^2}\frac{\partial W_2}{\partial x}+\frac{\partial U_2}{\partial x}\frac{\partial^2 W_2}{\partial x^2}-\frac{\alpha_T^B.\Delta T}{2}\frac{\partial^2 W_2}{\partial x^2}\right)\\
&-B_{11B}\left(\frac{\partial W_2}{\partial x}\frac{\partial^2 \Psi_2}{\partial x^2}+\frac{\partial^2 W_2}{\partial x^2}\frac{\partial \Psi_2}{\partial x}\right)-k_s A_{55B}\left(\frac{\partial^2 W_2}{\partial x^2}+\frac{\partial \Psi_2}{\partial x}\right)\\
&-2h_{11}h_f^B\left(\frac{\partial \phi_2}{\partial x}\frac{\partial^2 W_2}{\partial x^2}+\frac{\partial^2 \phi_2}{\partial x^2}\frac{\partial W_2}{\partial x}\right)\\
&+K_1 A_{55B}\left(\begin{array}{l}\left(\frac{\partial^2 W_2}{\partial x^2}\right)^3+4\frac{\partial W_2}{\partial x}\frac{\partial^2 W_2}{\partial x^2}\frac{\partial^3 W_2}{\partial x^3}+\left(\frac{\partial W_2}{\partial x}\right)^2\frac{\partial^4 W_2}{\partial x^4}\\ +2\frac{\partial^2 U_2}{\partial x^2}\frac{\partial^3 W_2}{\partial x^3}+3\frac{\partial^3 U_2}{\partial x^3}\frac{\partial^2 W_2}{\partial x^2}+\frac{\partial^4 U_2}{\partial x^4}\frac{\partial W_2}{\partial x}\end{array}\right)\\
&+K_1 B_{55B}\left(\frac{\partial W_2}{\partial x}\frac{\partial^4 \Psi_2}{\partial x^4}+\frac{\partial^2 W_2}{\partial x^2}\frac{\partial^3 \Psi_2}{\partial x^3}\right)+K_2 A_{55B}\left(\frac{\partial^4 W_2}{\partial x^4}+2\frac{\partial^3 \Psi_2}{\partial x^3}\right)\\
&+K_3 A_{55B}\left(\frac{\partial^4 W_2}{\partial x^4}-\frac{\partial^3 \Psi_2}{\partial x^3}\right)+k_{w3}W_2-G_{p3}\frac{\partial^2 W_2}{\partial x^2}+k_{w2}\left(W_2-W_1\right)\\
&-G_{p2}\left(\frac{\partial^2 W_2}{\partial x^2}-\frac{\partial^2 W_1}{\partial x^2}\right)+I_{0B}\frac{\partial^2 W_2}{\partial t^2}-0
\end{aligned}
\qquad \text{(C-2)}
$$

$\delta \Psi_2$:

$$
\begin{aligned}
&-D_{11B}\frac{\partial^2 \Psi_2}{\partial x^2}-B_{11B}\left(\frac{\partial^2 U_2}{\partial x^2}+\frac{\partial W_2}{\partial x}\frac{\partial^2 W_2}{\partial x^2}\right)+k_s A_{55B}\left(\frac{\partial W_2}{\partial x}+\Psi_2\right)\\
&+K_1 B_{55B}\left(\frac{\partial^4 \Psi_2}{\partial x^4}+3\frac{\partial^2 W_2}{\partial x^2}\frac{\partial^3 W_2}{\partial x^3}+\frac{\partial W_2}{\partial x}\frac{\partial^4 W_2}{\partial x^4}\right)+K_1 D_{55B}\frac{\partial^4 \Psi_2}{\partial x^4}\\
&-K_2 A_{55B}\left(2\frac{\partial^3 W_2}{\partial x^3}+4\frac{\partial^3 \Psi_2}{\partial x^2}\right)+K_3 A_{55B}\left(\frac{\partial^3 W_2}{\partial x^3}-\frac{\partial^2 \Psi_2}{\partial x^2}\right)\\
&+I_{2B}\frac{\partial^2 \Psi_2}{\partial t^2}+I_{1B}\frac{\partial^2 U_2}{\partial t^2}-0
\end{aligned}
$$

$\delta \phi_2$:

$$
-h_{11}h_f^B\left(\frac{\partial^2 U_2}{\partial x^2}+2\frac{\partial^2 W_2}{\partial x^2}\frac{\partial W_2}{\partial x}\right)+2\in_{11} h_f^B \phi_{2,x}-0
$$

Appendix D

Substituting Eq. (24) into Eqs. (C-1) and (C-2), the dimensionless governing equations of motion for both sandwich beams are derived as the following form

For CNTRC-SB:

$$a_{11C}\left(\frac{\partial^2 u_1}{\partial\zeta^2}+\frac{1}{\eta}\frac{\partial w_1}{\partial\zeta}\frac{\partial^2 w_1}{\partial\zeta^2}\right)-\hat{K}_1 a_{55C}\left(\frac{\partial^4 u_1}{\partial\zeta^4}+\frac{3}{\eta}\frac{\partial^2 w_1}{\partial\zeta^2}\frac{\partial^3 w_1}{\partial\zeta^3}+\frac{1}{\eta}\frac{\partial w_1}{\partial\zeta}\frac{\partial^4 w_1}{\partial\zeta^4}\right)$$
$$+b_{11C}\frac{\partial^2\psi_1}{\partial\zeta^2}+\hat{q}_{11}\left[\frac{\partial^3 u_1}{\partial\zeta^3}+\frac{2}{\eta}\left[\left(\frac{\partial^2 w_1}{\partial\zeta^2}\right)^2+\frac{\partial w_1}{\partial\zeta}\frac{\partial^3 w_1}{\partial\zeta^3}\right]\right]-\hat{K}_1 b_{55C}\frac{\partial^4\psi_1}{\partial\zeta^4}=I_{0C}\frac{\partial^2 u_1}{\partial\tau^2}+\hat{I}_{1C}\frac{\partial^2\psi_1}{\partial\tau^2}$$

$$a_{11C}\left(\frac{3}{2}\left(\frac{1}{\eta}\right)^2\frac{\partial^2 w_1}{\partial\zeta^2}\left(\frac{\partial w_1}{\partial\zeta}\right)^2+\frac{1}{\eta}\frac{\partial^2 u_1}{\partial\zeta^2}\frac{\partial w_1}{\partial\zeta}+\frac{1}{\eta}\frac{\partial u_1}{\partial\zeta}\frac{\partial^2 w_1}{\partial\zeta^2}-\frac{\alpha_T^C.\Delta T}{2}\frac{\partial^2 w_1}{\partial\zeta^2}\right)$$
$$-b_{11C}\left[\frac{1}{\eta}\frac{\partial w_1}{\partial\zeta}\frac{\partial^2\psi_1}{\partial\zeta^2}+\frac{1}{\eta}\frac{\partial^2 w_1}{\partial\zeta^2}\frac{\partial\psi_1}{\partial\zeta}\right]+k_s a_{55C}\left(\frac{\partial w_1}{\partial\zeta}+\eta\frac{\partial\psi_1}{\partial\zeta}\right)$$
$$+\hat{q}_{11}\left[\frac{1}{\eta}\frac{\partial^2 u_1}{\partial\zeta^2}\frac{\partial^2 w_1}{\partial\zeta^2}+\frac{2}{\eta^2}\frac{\partial w_1}{\partial\zeta}\left(\frac{\partial^2 w_1}{\partial\zeta^2}\right)^2+\frac{1}{\eta}\left(\frac{\partial u_1}{\partial\zeta}\right)^3\frac{\partial w_1}{\partial\zeta}+\frac{2}{\eta^2}\left(\frac{\partial w_1}{\partial\zeta}\left(\frac{\partial^2 w_1}{\partial\zeta^2}\right)^2+\frac{\partial^3 w_1}{\partial\zeta^3}\left(\frac{\partial w_1}{\partial\zeta}\right)^2\right)\right] \quad \text{(D-1)}$$
$$-\hat{K}_1 a_{55C}\left[\begin{array}{l}\frac{1}{\eta^2}\left(\frac{\partial^2 w_1}{\partial\zeta^2}\right)^3+\frac{4}{\eta^2}\frac{\partial w_1}{\partial\zeta}\frac{\partial^2 w_1}{\partial\zeta^2}\frac{\partial^3 w_1}{\partial\zeta^3}+\frac{1}{\eta^2}\left(\frac{\partial w_1}{\partial\zeta}\right)^2\frac{\partial^4 w_1}{\partial\zeta^4}\\ +\frac{4}{\eta^2}\frac{\partial w_1}{\partial\zeta}\frac{\partial^2 w_1}{\partial\zeta^2}\frac{\partial^3 w_1}{\partial\zeta^3}+\frac{3}{\eta}\frac{\partial^3 u_1}{\partial\zeta^3}\frac{\partial^2 w_1}{\partial\zeta^2}+\frac{2}{\eta}\frac{\partial^2 u_1}{\partial\zeta^2}\frac{\partial^3 w_1}{\partial\zeta^3}+\frac{1}{\eta}\frac{\partial^4 u_1}{\partial\zeta^4}\frac{\partial w_1}{\partial\zeta}\end{array}\right]$$
$$-\hat{K}_1 b_{55C}\left[\frac{1}{\eta}\frac{\partial w_1}{\partial\zeta}\frac{\partial^4\psi_1}{\partial\zeta^4}+\frac{1}{\eta}\frac{\partial^2 w_1}{\partial\zeta^2}\frac{\partial^3\psi_1}{\partial\zeta^3}\right]-K_2 a_{55C}\left(\frac{\partial^4 w_1}{\partial\zeta^4}+2\eta\frac{\partial^3\psi_1}{\partial\zeta^3}\right)-\hat{K}_3 a_{55C}\left(\frac{\partial^4 w_1}{\partial\zeta^4}-\eta\frac{\partial^3\psi_1}{\partial\zeta^3}\right)$$
$$-\hat{k}_{w1}w_1+\hat{G}_{p1}\frac{\partial^2 w_1}{\partial\zeta^2}-\hat{k}_{w2}\left(w_1-w_2\right)+\hat{G}_{p2}\left(\frac{\partial^2 w_1}{\partial\zeta^2}-\frac{\partial^2 w_2}{\partial\zeta^2}\right)-=\hat{I}_{0C}\frac{\partial^2 w_1}{\partial\tau^2}$$

$$
\begin{aligned}
&d_{11B}\frac{\partial^2\psi_1}{\partial\zeta^2}+b_{11B}\left(\frac{\partial^2 u_1}{\partial\zeta^2}+\frac{1}{\eta}\frac{\partial w_1}{\partial\zeta}\frac{\partial^2 w_1}{\partial\zeta^2}\right)-k_s a_{55B}\eta^2\left(\frac{1}{\eta}\frac{\partial w_1}{\partial\zeta}+\psi_1\right)\\
&-\hat{K}_1 a_{55B}\left(\frac{\partial^4 u_1}{\partial\zeta^4}+\frac{3}{\eta}\frac{\partial^2 w_1}{\partial\zeta^2}\frac{\partial^3 w_1}{\partial\zeta^3}+\frac{1}{\eta}\frac{\partial w_1}{\partial\zeta}\frac{\partial^4 w_1}{\partial\zeta^4}\right)\\
&-K_1 d_{55B}\frac{\partial^4\psi_1}{\partial\zeta^4}+\hat{K}_2 a_{55B}\eta^2\left(\frac{2}{\eta}\frac{\partial^3 w_1}{\partial\zeta^3}+4\frac{\partial^2\psi_1}{\partial\zeta^2}\right)-K_3 a_{55B}\eta\left(\frac{\partial^3 w_1}{\partial\zeta^3}-\eta\frac{\partial^2\psi_1}{\partial\zeta^2}\right)\\
&=\hat{I}_{2C}\frac{\partial^2\psi_1}{\partial\tau^2}+I_{1B}\frac{\partial^2 u_1}{\partial\tau^2}
\end{aligned}
\tag{D-1}
$$

For BNNTRC-SB:

$$
\begin{aligned}
&a_{11B}\left(\frac{\partial^2 u_2}{\partial\zeta^2}+\frac{1}{\eta}\frac{\partial w_2}{\partial\zeta}\frac{\partial^2 w_2}{\partial\zeta^2}\right)-\hat{K}_1 a_{55B}\left(\frac{\partial^4 u_2}{\partial\zeta^4}+\frac{3}{\eta}\frac{\partial^2 w_2}{\partial\zeta^2}\frac{\partial^3 w_2}{\partial\zeta^3}+\frac{1}{\eta}\frac{\partial w_2}{\partial\zeta}\frac{\partial^4 w_2}{\partial\zeta^4}\right)\\
&+b_{11B}\frac{\partial^2\psi_2}{\partial\zeta^2}+\hat{h}_{11}\left[\frac{\partial^3 u_2}{\partial\zeta^3}+\frac{2}{\eta}\left[\left(\frac{\partial^2 w_2}{\partial\zeta^2}\right)^2+\frac{\partial w_2}{\partial\zeta}\frac{\partial^3 w_2}{\partial\zeta^3}\right]\right]-\hat{K}_1 b_{55C}\frac{\partial^4\psi_2}{\partial\zeta^4}=I_{0B}\frac{\partial^2 u_2}{\partial\tau^2}+\hat{I}_{1B}\frac{\partial^2\psi_2}{\partial\tau^2}
\end{aligned}
\tag{D-2}
$$

$$
\begin{aligned}
&a_{11B}\left(\frac{3}{2}\left(\frac{1}{\eta}\right)^2\frac{\partial^2 w_2}{\partial\zeta^2}\left(\frac{\partial w_2}{\partial\zeta}\right)^2+\frac{1}{\eta}\frac{\partial^2 u_2}{\partial\zeta^2}\frac{\partial w_2}{\partial\zeta}+\frac{1}{\eta}\frac{\partial u_2}{\partial\zeta}\frac{\partial^2 w_2}{\partial\zeta^2}-\frac{\alpha_T^{(2)}.\Delta T}{2}\frac{\partial^2 w_2}{\partial\zeta^2}\right)\\
&-b_{11B}\left[\frac{1}{\eta}\frac{\partial w_2}{\partial\zeta}\frac{\partial^2\psi_2}{\partial\zeta^2}+\frac{1}{\eta}\frac{\partial^2 w_2}{\partial\zeta^2}\frac{\partial\psi_2}{\partial\zeta}\right]+k_s a_{55B}\left(\frac{\partial^2 w_2}{\partial\zeta^2}+\eta\frac{\partial\psi_2}{\partial\zeta}\right)\\
&+\hat{h}_{11}\left[\begin{array}{l}\frac{1}{\eta}\frac{\partial^2 u_2}{\partial\zeta^2}\frac{\partial^2 w_2}{\partial\zeta^2}+\frac{2}{\eta^2}\frac{\partial w_2}{\partial\zeta}\left(\frac{\partial^2 w_2}{\partial\zeta^2}\right)^2\\+\frac{1}{\eta}\left(\frac{\partial u_2}{\partial\zeta}\right)^3\frac{\partial w_2}{\partial\zeta}+\frac{2}{\eta^2}\left(\frac{\partial w_2}{\partial\zeta}\left(\frac{\partial^2 w_2}{\partial\zeta^2}\right)^2+\frac{\partial^3 w_2}{\partial\zeta^3}\left(\frac{\partial w_2}{\partial\zeta}\right)^2\right)\end{array}\right]\\
&-\hat{K}_1 a_{55B}\left[\begin{array}{l}\frac{1}{\eta^2}\left(\frac{\partial^2 w_2}{\partial\zeta^2}\right)^3+\frac{4}{\eta^2}\frac{\partial w_2}{\partial\zeta}\frac{\partial^2 w_2}{\partial\zeta^2}\frac{\partial^3 w_2}{\partial\zeta^3}+\frac{1}{\eta^2}\left(\frac{\partial w_2}{\partial\zeta}\right)^2\frac{\partial^4 w_2}{\partial\zeta^4}\\+\frac{4}{\eta^2}\frac{\partial w_2}{\partial\zeta}\frac{\partial^2 w_2}{\partial\zeta^2}\frac{\partial^3 w_2}{\partial\zeta^3}+\frac{3}{\eta}\frac{\partial^3 u_2}{\partial\zeta^3}\frac{\partial^2 w_2}{\partial\zeta^2}+\frac{2}{\eta}\frac{\partial^2 u_2}{\partial\zeta^2}\frac{\partial^3 w_2}{\partial\zeta^3}+\frac{1}{\eta}\frac{\partial^4 u_2}{\partial\zeta^4}\frac{\partial w_2}{\partial\zeta}\end{array}\right]\\
&-\hat{K}_1 b_{55B}\left[\frac{1}{\eta}\frac{\partial w_2}{\partial\zeta}\frac{\partial^4\psi_2}{\partial\zeta^4}+\frac{1}{\eta}\frac{\partial^2 w_2}{\partial\zeta^2}\frac{\partial^3\psi_2}{\partial\zeta^3}\right]-K_2 a_{55B}\left(\frac{\partial^4 w_2}{\partial\zeta^4}+2\eta\frac{\partial^3\psi_2}{\partial\zeta^3}\right)\\
&-\hat{K}_3 a_{55B}\left(\frac{\partial^4 w_2}{\partial\zeta^4}-\eta\frac{\partial^3\psi_2}{\partial\zeta^3}\right)\\
&-\hat{k}_{w3}w_2+\hat{G}_{p3}\frac{\partial^2 w_2}{\partial\zeta^2}-\hat{k}_{w2}(w_2-w_1)+\hat{G}_{p2}\left(\frac{\partial^2 w_1}{\partial\zeta^2}-\frac{\partial^2 w_2}{\partial\zeta^2}\right)-=\hat{I}_{0B}\frac{\partial^2 w_2}{\partial\tau^2}
\end{aligned}
\tag{D-2}
$$

$$
\begin{aligned}
&d_{11B}\frac{\partial^2\psi_2}{\partial\zeta^2}+b_{11B}\left(\frac{\partial^2 u_2}{\partial\zeta^2}+\frac{1}{\eta}\frac{\partial w_2}{\partial\zeta}\frac{\partial^2 w_2}{\partial\zeta^2}\right)-k_s a_{55B}\eta^2\left(\frac{1}{\eta}\frac{\partial w_2}{\partial\zeta}+\psi_2\right)\\
&-\hat{K}_1 a_{55B}\left(\frac{\partial^4 u_2}{\partial\zeta^4}+\frac{3}{\eta}\frac{\partial^2 w_2}{\partial\zeta^2}\frac{\partial^3 w_2}{\partial\zeta^3}+\frac{1}{\eta}\frac{\partial w_2}{\partial\zeta}\frac{\partial^4 w_2}{\partial\zeta^4}\right)\\
&-\hat{K}_1 d_{55B}\frac{\partial^4\psi_2}{\partial\zeta^4}+\hat{K}_2 a_{55B}\eta^2\left(\frac{2}{\eta}\frac{\partial^3 w_2}{\partial\zeta^3}+4\frac{\partial^2\psi_2}{\partial\zeta^2}\right)-K_3 a_{55B}\eta\left(\frac{\partial^3 w_2}{\partial\zeta^3}-\eta\frac{\partial^2\psi_2}{\partial\zeta^2}\right)\\
&=\hat{I}_{2B}\frac{\partial^2\psi_2}{\partial\tau^2}+I_{1B}\frac{\partial^2 u_2}{\partial\tau^2}
\end{aligned}
$$